CONSTRUCTION AND TESTING OF A REINFORCED CONCRETE HYPERBOLIC COOLING TOWER MODEL

by

KARL CHIA-CHANG CHIEN

B.S., National College of Marine Science and Technology, 1971

A MASTER'S THESIS

submitted in partial fulfillment of the

requirements for the degree

MASTER OF SCIENCE

Department of Civil Engineering

KANSAS STATE UNIVERSITY
Manhattan, Kansas

1983

Approved by:

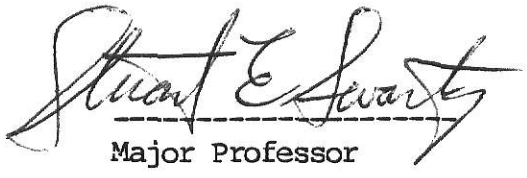

Major Professor

Contents

	Page
List of Tables	ii
List of Figures	iii
Chapter I. Introduction	1
Chapter II. Literature Review	3
Chapter III. Shell Shape and Construction	7
Chapter IV. Shell Test	18
Chapter V. Test Results	21
Chapter VI. Meridional Imperfection	29
Chapter VII. Conclusions	32
References	34
Appendix I. Tables	36
Appendix II. Figures	43
Appendix III. Computer Program	61
Appendix IV. Notations	68
Acknowledgements	71
Abstract	73

List of Tables

		Page
1.	Properties of Micro-Concrete and Reinforcing	37
2.	Cylinder Test Log	38
3.	Deviation From Ideal Geometry	39
4.	Shell Thicknesses	40
5.	Experimental Bending Moments and Forces at Maximum Load	41
6.	Predicted Pressures and Internal Forces Associated With Possible Local Buckling	42

List of Figures

		Page
1.	Cylinder Tests	44
2.	Formwork	45
3.	Concrete Pump	46
4.	Shell No. 1 With Deflection Gage Support Beam	47
5.	Meridional Locations for Thickness, Geometry Displacement and Strain Data	48
6.	Circumferential Locations for Thickness, Geometry and Displacement Data	49
7.	Strain at Top of Shell Just Below Ring, Line H	50
8.	Strain at Throat, Line H	51
9.	Strain at Throat, Line E	52
10.	Strain at Throat, Line B	53
11.	Strain Four Feet Below Throat, Line H	54
12.	Strain at Base, Line H	55
13.	Measured and Theoretical Support Column Loads	56
14.	Deflection Profiles	57
15.	Failed Region	58
16.	Outside View of Hole	59
17.	Inside View of Hole	60

CHAPTER I

INTRODUCTION

In a thermal power station, heated steam drives the turbogenerator, which produces electric energy. To create an effective heat sink at the end of this process, the steam is condensed and recycled into the boiler. This requires a large amount of cooling water, which is heated and may be recooled artificially in a cooling tower.

In order to avoid thermal pollution of rivers, lakes, and seashores, natural draft cooling towers are effective and popular corrective measures. These structures are able to balance environmental factors, investment and operating costs of the power station with the demands of a reliable electric energy supply.

Hyperbolic, natural-draft cooling towers continue to be among the largest reinforced concrete thin-shell structures being built. Towers up to 600 feet tall are being designed and constructed in both Europe and North America, and a recent conference focused on the potential of even larger shells (17). For those cooling tower shells that have been built, although their design and construction have mainly followed approved rules of craftsmanship, at least five completed or nearly completed cooling towers have failed or been damaged by wind storms(3).

In the design of large thin shells, stability is a vital concern. International research activities have been intensified and concentrated on

dynamic effects and stability effects. In the past 10 years many cooling tower research projects, public and private, have been carried out. However, there is a lack of physical evidence regarding the stability of these reinforced concrete, wall-type shells under horizontal loads. Few buckling experiments have been conducted on concrete or micro-concrete cylinders, hyperboloids, or toroids subjected to lateral axisymmetric or asymmetric pressures. The only relevant tests are limited in number and have been conducted with metal or plastic models(6). For concrete or micro-concrete wall-type shell models, tests would have a closer similarity to reinforced concrete prototypes than metal or plastic models.

The experiment the author has carried out was concerned with a micro-concrete hyperboloid of revolution, wall-type shell model. The test was conducted for a simple, non-offset, hyperboloidal shell with essentially uniform thickness, 0.5 in.(1.27 cm), 12 ft.(3.66 m) high. The shell was 9.33 ft. (2.84 m) and 6 ft.(1.83 m) in diameter at the base and throat respectively.

The objective of this research was to obtain experimental evidence on the buckling behavior of this type of concrete shell. The construction, testing, data collection and analysis will be presented in detail. The effect of imperfections also be discussed.

CHAPTER II

LITERATURE REVIEW

In Ref.(23), Vandepitte and Rathe tested spherical concrete shells subjected to uniform radial pressure. Their results were: The buckling phenomenon is a local one. It seems that the thickness in the vicinity of the buckle should be taken into account. But, the buckle position was not necessarily the place of minimum thickness. Minor thickness variations do not significantly affect the buckling load. The buckling position occurs nearly always between 2/3 of radius from the center and the edge. The repeatability of the constant failure form is a punched hole, almost a perfect circle, with a radius of approximately 6.69 in.(17 cm).

Mungan(19) tested several hyperboloidal shells 32.2 in.(82 cm) high, 15.7 in.(40 cm) diameter at the throat, with nominal thickness, about 0.08 in.(2mm). He used a cold mix of epoxy resin with hardener as material and reached the following conclusion: The buckling of hyperboloidal shells depends mainly on the wall thickness, local imperfections, and the stress state acting in the model. The effect of local imperfections is much more than the effect of the edge conditions. According to him, Mungan also presented a nondimensional interaction formula for estimating the buckling load(19).

So far, there exists only a small body of experimental results relevant to the problem of stability of large, concrete hyperboloids subject to wind loadings. Three categories of analysis approach are

identified (3): (a). Scaled-up wind tunnel tests (13). (b).Methods based on axisymmetric experiments(19), use of equivalent axisymmetric loadings (8,11) and use of equivalent axisymetric stresses (2,7,8,9). (c).Methods not based on axisymmetry(20).

No single approach is universally accepted or used. Some designers and researchers advocate a local buckling criterion as opposed to a global stability treatment. Some other differences include: bifurcation predictions as opposed to limit-point analyses, reduced shell theories to obtain lower bounds rather than full shell theories, and axisymmetric simplifications instead of full nonaxisymmetric methods. It is assumed that bifurcation calculations with well-verified methods can provide an acceptable estimate of buckling of wind loaded hyperboloids for routine design purposes. The prediction of buckling for the design of cooling tower shells could be improved by more experimental evidence for the verification and comparison of prediction methods.

In Billington and Harris' paper(6), cooling tower shells are classified as wall type shells because the orientation of the shells is essentially vertical and the primary loads for buckling are horizontal. It is, indeed, wind loadings that govern the design of practically all cooling towers, and the stability of the shells under these relatively short duration loads is the major concern of the designer when buckling safety is assessed.

Prediction capabilities for the stability of cooling tower shells have been presented by Croll and Chilver(11), Billington(5), Abel and Billington

(1), and Cole, Abel, and Billington (8). In the five years since the last of these, further contributions have been recorded. In particular, new experimental and analytical results are available and more extensive efforts have been made to correlate analytical and numerical predictions with experiments.

In general, there is a lack of physical evidence regarding the stability of reinforced concrete, wall-type shells under horizontal load. No buckling experiments have been conducted on concrete or microconcrete hyperboloids, or toroids subjected to lateral axisymmetric or asymmetric pressures. The only relevant tests are limited in number and have been conducted with metal or plastic models (6).

Interest in the effects of geometry imperfections in hyperbolic cooling tower design has increased since the collapse of the 350 ft.(107 m) Ardeer tower in Scotland September 1973. In Ref.(10), the shape of imperfection is assumed to be a combination of circular arcs. For the influence of meridional imperfections, two approaches to the simulation of axi-symmetric meridionally imperfect shells have been used by Croll and Kemp (12). In the first approach, the geometry of the imperfect tower is modelled exactly as a series of piece-wise continuous second order shells of revolution, and the appropriate equations for shell bending are solved using a finite difference discretisation. In the second approach the geometric imperfection is simulated by a normal pressure distribution chosen so that it is staticlly eqivalent to the out-of-balance forces that would be present when the membrane stresses of the perfect shell. In their

study, a significant increase in hoop stresses is recognized as a major effect of imperfections.

In a subsequent paper (10), Croll, Kaleli and Kemp have analyzed a cooling tower with axisymmetric imperfections using the bending theory. This analysis yields, both the imperfection hoop force and the meridional bending moment. They assume that flexural failure due to the imperfection generated meridional moments will not precipitate collapse, but that the shell has sufficient ductility to enable a redistribution from bending to membrane action to occur.

In Ref.(15), Gupta and Al-Dabbagh state that the meridional moment plays an important role in the safety of the tower. A general meridional shape of imperfection is assumed, which becomes the straight line or the circular shape as two extremes depending on the value of a parameter "C" (15). Simple expressions for the maximum possible imperfection hoop force and meridional moments have been obtained and will be discussed later.

CHAPTER III

SHELL SHAPE AND CONSTRUCTION

What is the best form of the meridional curve? A properly shaped cooling tower shell remains in a state of complete compression for most of its lifetime. However in the case of severe storms the compression in the flanks of the tower will increase dramatically and also will decrease or change into tension near the windward meridian. Thus the shell must resist tensile forces, as well as instability effects due to compression.

A general hyperboloid of revolution may be described by:

$$(R - R_o)^2 / a^2 - z^2 / b^2 = 1$$

or

$$R - R_o = a \sqrt{1 + z^2/b^2}$$

or

$$R = R_o + a \sqrt{1 + z^2/b^2} \qquad \text{---------- (1)}$$

Apart from considerations of thermodynamics, the most economical shape for a cooling tower is often questioned, varying the basic sizes within certain limits. Should preference be given to slim or compact structures? Which is the best form of the meridional curve?

To answer these or similar questions, a parametric study was carried out by Zerna, Haj-Issa, Lehmkamper and Mungan (17) in which three types of cooling towers were compared. They are different in height but are equal

THIS BOOK
CONTAINS
NUMEROUS PAGES
WITH THE ORIGINAL
PRINTING BEING
SKEWED
DIFFERENTLY FROM
THE TOP OF THE
PAGE TO THE
BOTTOM.

THIS IS AS RECEIVED
FROM THE
CUSTOMER.

in volume and their base diameters are nearly equal. Thus the thermal efficiency of the towers is nearly identical. For each tower a variation of the analytic form of the meridional curve using the parameter R_o, in Eq.(1), was carried out. In Eq.(1), R_o=0 describes a pure non-offset hyperbola rotating about its axis. For values of R_o greater (smaller) than zero, the axis of the hyperbola lies between (outside) the meridional curve and the central axis. This parameter R_o significantly influences the response of the tower.

The results of the investigation demonstrated that there is no advantage to designing slim or compact towers. Slim cooling towers are expected to have a slightly higher buckling safety, but their lowest natural frequencies are smaller. Thus, compact towers are affected less intensely by atmospheric turbulence. In any case, cooling towers with large negative values of the parameter R_o behave best: They show the most uniformly curved meridians leading to the highest facters of buckling safety and natural frequencies. However, for simplification of construction, in the experiment reported herein, the model was constructed to be a simple, non-offset hyperboloid, R_o=0, with thickness, 0.5 in.(12.7 mm), 12ft. (3.66 m) high, 9.33 ft.(2.84 m) and 6 ft.(1.83 m) in diameter at the base and throat respectively. The shell was cast using microconcrete and was reinforced by wires 0.105 in. (2.7 mm) in diameter.

MODEL MATERIALS

The thin-walled construction which was to be used required that a model concrete consisting of sand (passing #16 sieve), cement and water be used. The development of this micro concrete mix had two considerations:

1. The mix should have properties when hardened similar to the prototype concrete commonly used in these shells.
2. The mix should be capable of being pumped.

In development of the mix, considerable effort was made to standardize procedures for making, placing, curing and testing specimens. A total of thirty-five trial mixes were used to evaluate slump, density, and ultimate strength as a function of the aggregate/cement and water/cement ratios.

In addition, a unique technique for placing strain gages on the cylinders (1 in. X 2 in.) while still in the curing cycle was developed. A description of this technique and results obtained -- which showed excellent repeatability are contained in Reference (18).

The final mix proportions which met the two requirements of similitude and pumpability are given in Table 1.

Following the concept described in Reference (14) the shell was cast in three lifts. The casting dates and results of compressive tests on 3 in.X 6 in.(75 X 150 mm) cylinders which were cured in their molds adjacent to the shell (variable temperature and humidity environment) are given in Table 2.

Uniaxial stress-strain curves for cylinders from lifts one and two are displayed in Fig.1. These curves show remarkable similarity in shape and magnitudes to those obtained from the tests on 1 in. X 2 in. (25 X 50mm) cylinders cured in 100% humidity which are given in Reference (18).

The average value of cylinder compressive strength is taken from the cylinders tested at 200 plus days and is f_c' = 6280 psi (43.3 MPa). However, the values of strain at failure ε_o and secant modulus of elasticity E_c are arbitrarily taken from the data for the first lift concrete (tested at 221 days) and are: ε_o = 0.00358 in./in. (m/m) and E_c = 3.62 X 10^6 psi (24.9 GPa) since the failed region of the shell was in the first lift. The value of Poisson's Ratio obtained from the cylinder test was 0.16 and the split cylinder tensile strength (again on first lift cylinder) was 660 psi (4.5 MPa).

Reinforcing in the shell consisted of 0.105 in. (2.7 mm) diameter steel wire placed in two directions along the ruling lines nominally in the middle surface of the shell. The shell geometry and location of ruling lines are given in Reference (14). There were forty wires evenly spaced in each direction giving a nominal steel ratio based on a 0.5 in.(13 mm) thick shell of 0.35%. The wire spacings were 5.7 in. (14 cm) at the throat and 8.8 in.(22 cm) at the base. Thus the spacing was from 15 to 18 times the nominal shell thickness. This violates the maximum spacing of twice the shell thickness recommended by ACI-ASCE Committee 334 (4) and may have contributed to the mode of failure that was experienced.

The top of the shell was thickened into a ring two inches wide and one inch deep(50X25mm) reinforced with six wires as described in Reference(14).

The wire was annealed and then straightened. Nevertheless, the average yield strength of tensile specimens was f_y = 81.9 ksi (564 MPa). The modulus of elasticity, E_s = 29.8 X 10^6 psi (206 GPa).

CONSTRUCTION OF SHELL

The sequence for the model construction is the following:

I. Assemble inner form and apply bond breaking compound (grease).

Both of the inner and outer forms were cut into three lifts. For each lift, the form was also cut into six panels. Several pieces of balsa wood, 1" X 3", (2.54 cm X 7.6 cm), 1/16" (1.6 mm) in thickness were glued around each panel for the compensation of loss of material due to saw blade width when the pannel was cut. When assembling each lift a special clamp was needed to join temporarily two panels. This clamp is shown in Fig.2 . An attempt was made to assure that the geometry was as good as it was before the lift was cut. The lifts were fastened by screwing metal strips between two panels vertically and horizontally, after the next lift was finished, as shown in Fig.2. The vertical metal strips were bent by 10° along the narrow side in accordance with the circumferencial curvature. There are two functions of the metal strips: 1. Connect and fasten between panels. 2. Seal the mortar as well as water when concrete is cast. After the inner form was assembled, the gaps between panels were taped and grease was applied all around the forms as a bond breaking compound to facilitate tear down of the panels after curing of the concrete.

II. Assemble reinforcing wires.

The geometry and length of the reinforcing wires were described in Reference (14). The reinforcing wires include those in a reinforced concrete beam at the top of the shell. Note that the shell wires were

threaded at the top and bottom and attached to the rings with nuts. The torque applied on the nuts was controlled and the tension on the wire checked by eye. This was done in an attempt to ensure that every wire was equally prestressed. The wires need enough prestress to overcome sagging due to selfweight. The top ring of the support frame was aligned to make sure the shell geometry was correct. The tension in each wire was rechecked and adjusted as necessary.

III. Assemble first lift of greased outer form.

Like the inner forms, the balsa wood was attached along the sawn edge and metal strips were screwed between two panels. Besides these, spacers were needed to control the shell thickness to be 1/2in.(13mm). Spacer pieces were made of aluminum tubing 1/2 in. (13 mm) long and divided into two groups, compressive type and tensile type. For the compressive type, a bolt goes through the outer form and aluminum tubing is attached to the spacer on the outer form by nuts. The compressive spacer was designed to be against the inner form to prevent the wall from being less than 1/2 in.(13 mm). For the tensile type, a bolt goes through both forms as well as the aluminum tubing which ties both forms by two nuts beyond the forms. The tensile spacer was designed to hold the forms from coming apart when concrete was cast. On the ends of both types of spacers, washers were needed to prevent punching of the form wall. Both types of spacer were placed at the four corners and interior locations to assure proper spacing between forms. After casting the first lift it was determined that the outer form needed to be wrapped with four cables and

tightened with turn buckles at different levels to resist the hydraulic force which tended to bulge and separate the forms.

IV. Fill lower lift with pumped concrete.

The concrete pump is shown in Fig.3. The equipment used is described more fully in Reference (14). Briefly, it consisted of an auger-drive pump with a feed hopper and attached lines and fittings. Besides the vibration during casting, the first lift was filled about one third full. Pouring was stopped and the form was vibrated thoroughly. Then the formed was filled again and vibrated. It was found that due to large fluid friction, if vibration commences after pouring has been completed, large voids may still exist. After the lower lift was finished the top edge was cleaned, and additional reinforcement was placed. These were 6 in.(15.2 cm) long pieces of reinforcing wire,3 in.(7.6 cm) inserted into the concrete and 3 in.(7.6 cm) into the air for the connection to the next lifts which would be poured on a cold joint.

V. Repeat steps III and IV for the other lifts.

In placing the forms for the top lift, the top ring beam should be noted. The form design for the top ring beam was given in Ref.(14). It was composed of two pieces of deformed iron sheet, into which six slots were cut. These were bolted onto each top form. The elevation of the top beam can be adjusted by loosening those six bolts. Before the top lift was cast, those forms for the top beam were determined to be at the right elevation. For compatibility and sealing between the

two forms of the top beam, additional reinforcement was needed, masking tape was used for sealing.

VI. Form removing.

After curing, the inner molds of the top lift were removed first and necessary patching concrete was placed against the outer molds. Then, the outer molds for the top lift were removed and patching was done as necessary. This process was repeated for the 2nd and bottom lifts. The outer molds were fairly easy to remove - just cut the space bolts and separate carefully. But, for the inner molds, due to the curvature and thickness, a condition like a reverse wedge is produced. It was much more difficult to tear these down than the outer molds. So, when the inner molds were removed some damage was caused especially for the first panel of each lift.

VII. Concrete patching.

Due to the imperfection of the forms and incomplete vibration, the concrete could not be distributed uniformly between forms. This caused some holes and voids which needed concrete patching.

The properties of micro-concrete used for patching were the same as those used in the original mix but water was reduced by 20% to produce zero slump. In other words, the mix design of micro-concrete for patching is the same as given in Table 1 but the water was changed from 19.23 lbs (85.6 N) to 15.4 lbs (68.5 N) per cu. ft. of mix to get slump to be zero inch.

The concrete patching was done from the top inner lift to the bottom outer lift. First, the top inner forms were removed keeping

the outer forms as a support, and the concrete was placed against the outer forms. After curing, the top outer forms, were removed and the concrete troweled again as necessary. This process was repeated for the 2nd and the bottom lifts. It was possible to remove either all the inner or outer forms and then trowel the whole shell at the same time. However, the shell may fail because the dead weight of the forms may be large enough to collapse the shell before the holes have been patched.

Before patching, around the holes, the old concrete must be saturated by plasma of cement and water, or, the new concrete may not stick to the old concrete.

VIII. Cut reinforcment wire, install top plywood cover over the shell.

After the molds were taken off and concrete was patched, the reinforcement wires attached to the top steel ring had to be cut to get an independent shell. Because there are some prestress forces in the wires, the wires have to be cut across the diameter evenly to get the uniform stress distribution in the shell. The wire ends were ground and concrete mortar placed on the top beam to make the top surface very smooth.

The top cover was shown in Ref.(14). It is composed of two pieces of a semicircle made of 1/2 in.(12.7 mm) plywood and reinforced by a grid of 2" X 4" (50.8 mm X 101.6 mm) wooden beams. Rubber was bonded around the edge of the cover to provide better sealing between the cover and the concrete. The cover is heavy. A caulking compound was also used between the rubber and concrete shell top beam. Before the caulking compound was cured the top plate was placed and adjusted

to its correct position. After that, silicone sealer was used to seal all around the plate and the concrete top beam. After the silicone was cured hydrostone was troweled onto the silicone to fill up the triangular gap between edge of plate and top beam. The purpose of the hydrostone is to provide better and stronger sealing. A 2" X 4" (50.8 mm X 101.6 mm) wood beam was placed over the gap between the two semicircle plates. This was reinforced by a steel angle outside the shell and steel plate inside the shell. All pieces were bolted tightly together.

For shell No.1, the formwork was completely assembled to see how it would fit together and then the top two lifts of the outer form were removed. A photograph of the forms with all of the inner forms and two lifts of the outer forms in place is shown in Fig.2. Due to imperfections in the form surface, there were difficulties encountered in attempting to maintain the nominal shell thickness.

The construction sequence of assembling forms and pumping concrete as described above generally was followed.

Some problems were encountered in placing the first lift of concrete due to inexperience in using the equipment and coordinating manpower. Also, as mentioned previously it developed that there were insufficient form ties with the result being a considerable bulging and some separation of the forms. How serious this was became apparent later when thickness measurements were made.

Corrections made to succeeding pours included additional bracing on the forms and more form ties. The pours for the top two lifts were attained with little difficulty. Due to scheduling problems the lifts were poured about a week apart. To enhance the strength of the shell at the cold joints additional wires were placed in the plastic concrete of the previous pour at the joint.

Concrete and plywood are porous materials which are not air tight when they are only 1/2 in.(13 mm) thick. Three layers of perma-cure were sprayed on the concrete. Perma-cure is a membrane curing seal for concrete. Also, two layers of varnish were sprayed on the top and botton plates. Even then, the shell was not air tight. It was pressurized with compressed air, then, an emulsifier (Scothy), used to produce bubbles, was painted on the surface of concrete to find the major voids. The major voids were sealed with silicone. These spots are shown in Fig.4.

Finally, a low-shrink resin which was like that used in the form construction was applied. The resin was mixed with 3.5 cubic centimeters of catalyst per quart. The mixed resin was painted on the shell and then covered by Saran Wrap. There were at least 2 in.(5.1 cm) of overlap between two strips of Saran Wrap and their edges were taped to provide better sealing. The shell was finally ready to mount strain gages. The first shell is shown in Fig.4.

CHAPTER IV

SHELL TEST

STRAIN AND DISPLACEMENT INSTRUMENTATION

Locations for strain measurements, deflection measurements, geometry and thickness measurements are shown in Fig.5 and 6.

Electrical resistance foil strain gages which were temperature compensated were used. These were two element retangular rosettes with a gage length of 0.125 in.(3.18 mm) (Micro Measurement EA-06-125 TF-120). The gages were mounted, wired and protected following standard techniques. They were oriented to be parallel to the circumferential direction (even-numbered gages) and meridional direction (odd-numbered gages). All strain data was taken with a Vishay 220 data acquisition system.

Deflection measurements were taken from dial gages with a least reading of 0.001 in.(0.0254 mm) and travel of 2 in.(50 mm). These were mounted on a portable beam which could be moved to the various circumferential locations indicated in Fig.6. This support beam is shown in detail in Reference (14) and can be seen in Fig.4.

Geometry measurements were made from the shell surface to the back of the deflection gage support beam using a caliper and a ruler.

Thickness measurements were made after the shell was tested by drilling holes and measuring through these at the locations indicated in Fig.5 and 6.

Finally, strain gages were placed on the steel column which supported the center of the top cover (Reference 14) to determine the amount of load carried during the test.

LOADING EQUIPMENT AND TESTING PROCEDURE

Conceptually, loading the shell with uniform pressure is quite simple using a large capacity vacuum pump and a mercury manometer to indicate the pressure. The specific gravity of mercury is 847 lbs per cubic foot, 0.49 lbs per cubic in. Therefore 1 inch of mercury is equal to 0.49psi(3.37kpa).

In practice, problems were encountered with leakage which were rather severe and came primarily from three sources.

1. The shell itself leaked. As mentioned before, a number of solutions were attempted to seal the concrete. The approach that proved sucessful was to coat the shell surface with a thin layer of resin and hardener and attach plastic wrap to this.

2. The plywood surfaces of the top and bottom covers leaked. Again the resin and plastic wrap proved sufficiently air-tight.

3. Joints and connections leaked. These were sealed with different commercial compounds (liquid nail, etc.).

Because of the size of the shell and amount of surface area are involved, the process of isolating the leaks and providing corrective measures was rather lengthy. A considerable amount of time was spent in determining appropriate methods to use.

Additional problems were encountered when load was first applied successfully in that the plywood surfaces deflected sufficiently to open new leaks. These surfaces were further stiffened and leaks located and sealed.

The loading equipment consists primarily of a high vacuum, high capacity pump; lines and fittings; and a mercury manometer. The vacuum line has a shut off valve which allows a constant vacuum to be maintained.

The testing procedure was:

1. Initialize strain and dial gage data;
2. Apply load to desired level and maintain;
3. Record strain data and dial data;
4. Repeat steps 2 and 3.

No difficulties were encountered taking strain data. However, only a limited amount of deflection data was actually taken due to time constraints and inconsistencies in technique. This aspect of data acquisition is being revised at the present time.

CHAPTER V

TEST RESULTS

Measurements of deviation from the ideal geometry were taken at 132 locations. These consist of differences from the ideal shell horizontal radius to the outer surface at the locations indicated in Table 3 and Fig.5 and 6. It is seen that the maximum deviation in radius was sbout +_ 3%.

The percent deviation in a vertical distance along a meridian expressed as a slope S is significant only in a local sense. In this regard, since the locations at which measurements were made were spaced 12 in.(0.3 m) apart the slope was defined over three data points as

$$S = 2\Delta/H \times 100 \qquad \text{----------} \qquad (5\text{-}1)$$

where

$\Delta = dR_j - 1/2\ (dR_i + dR_k)$ = the net radial deviation of the shell surface over a gage length H = 24 in. and dR_i, dR_k = radial deviations at the ends of the gage length while dR_j is the radial deviation at the center of the gage length.

dR is the measured deviation from the ideal geometry indicated in Table 3, inward is positive; outward is negative.

The maximum values of S obtained by applying Eq.(5-1) to the data for each vertical line are given in Table 3. The overall maximum values of S are about +_ 4.5%.

For the geometric imperfection, if we take the thickness which will be described later into account, then :

$$D_{ij} = dR_{ij} + dt_{ij}/2$$

is the central line radial deviation from ideal geometry. In this, dt is the deviation of shell thickness from 0.5 in.(13 mm), i is the gage number, from 1-11, j is the line number, from A-L, ie., from 1-12.

For example :

At the throat, on line A :

$dR_{41} = -0.83$ $\qquad$ $dt_{41} = 0.6 - 0.5 = 0.1$

$$D_{41} = dR_{41} + dt_{41}/2$$
$$= -0.83 + 0.1/2$$
$$= -0.78$$

At the throat, on line C :

$dR_{43} = 0.67$ $\qquad$ $dt_{43} = 0.33 - 0.5 = -0.17$

$$D_{43} = dR_{43} + dt_{43}/2$$
$$= 0.67 - 0.17/2$$
$$= 0.585$$

And then

$$D_d(i,j) = D_{i+1,j} - (D_{i,j} + D_{i+2,j})/2$$

in which,

D_d is the imperfection out of round from the perfect shape in the radial direction. D_d will be used to calculate the hoop force and and meridional bending moment due to imperfection in next chapter.

Thus, the shell geometry is not as accurate as encountered in practice today. On the other hand, a scale factor of around 30 essentially precludes achievement of tolerances comparable to those required for the prototype.

SHELL THICKNESS

Thickness measurements at 138 locations were made after the shell was tested to failure by drilling holes at the locations indicated in Figs.5 and 6 including those adjacent to the strain gages. The thicknesses measured are displayed in Table 4.

The extremely large thicknesses in lift one along lines A, B, C, E, F, G, H, and some other locations in that lift are due to form bulging and separation which occured during vibration.

The other thicknesses are closer to the nominal value of 0.5 in.(13mm) but still show unacceptable variations. These variations are a function of the form surface itself but can be corrected for future models by additional surface finishing of the forms.

STRUCTURAL RESPONSE AND FAILURE

Strain versus load curves for the last test of the shell prior to failure (testing age 189 days from date of last pour and 14 days before test to failure) are presented in Figs.7-12. In general, the response is linear up to the maximum load of 3.0 psi (20.7 kpa) with no indication of buckling. The failure load was 3.1 psi (21.4 kpa). Also shown on the plots are theoretical curves based on membrane theory and converted to strains by

$$\varepsilon_\phi = (N_\phi - \mu N_\theta) / t E_c$$

$$\varepsilon_\theta = (N_\theta - \mu N_\phi) / t E_c \qquad \text{----------(5-2)}$$

where

ε, N are the strain and membrane force in either the meridional or circumferential directions respectively and t is the measured shell thickness at the gage location, and μ is Poisson's Ratio. The value of $\mu$was determined by the stress-strain test and is 0.16. The value of E_c was determined as the secant modulus to the stress-strain curve in Fig.1 and is 3.62×10^6 psi (24.9 GPa). In calculating N_ϕ , N_θ it was assumed the support column carried 5/9 the load from the top cover.

For the average strains, the curves presented indicate reasonable agreement with membrane theory amended by meridional imperfection which will be discussed in the next chapter. Values of shell forces and moments at the locations of the strain gages are given in Table 5 for the maximum load of 3.0 psi (20.7 kpa). The calculations of experimental bending moment and forces for Table 5 are :

$$\sigma_{i\theta} = E_c[(1-\mu)\,\varepsilon_{i\theta} + \mu\varepsilon_{i\phi}]/(1+\mu)(1-2\mu)$$

$$\sigma_{o\theta} = E_c[(1-\mu)\,\varepsilon_{o\theta} + \mu\varepsilon_{o\phi}]/(1+\mu)(1-2\mu)$$

$$N_\theta = (\sigma_{i\theta} + \sigma_{o\theta})\,t\,/\,2$$

$$M_\theta = t^2\,(\sigma_{o\theta} - \sigma_{i\theta})/6$$

Similarly

$$\sigma_{i\phi} = E_c[(1-\mu)\,\varepsilon_{i\phi} + \mu\varepsilon_{i\theta}]/(1+\mu)(1-2\mu)$$

$$\sigma_{o\phi} = E_c[(1-\mu)\,\varepsilon_{o\phi} + \mu\varepsilon_{o\theta}]/(1+\mu)(1-2\mu)$$

$$N_\phi = (\sigma_{i\phi} + \sigma_{o\phi})\,t\,/\,2$$

$$M_\phi = t^2\,(\sigma_{o\phi} - \sigma_{i\phi})/6$$

In which,

σ is the stress

ε is the strain, obtained from strain gage data

i is inner face of the shell

o is outer face of the shell

E_c is the secant modulus which is 3.62×10^6

μ is Poisson Ratio which is 0.16

N is membrane force, tension is positive

M is bending monemt, positive moment causes tension in the outer layer of the shell.

Some observations are that

1. At the three throat locations (90 ° apart circumferentially) the moments are quite small.
2. At these same locations the forces are not equal - hence the structural response is unsymmetrical.

3. At locations other than just below the top ring the circumferential (θ) forces predominate.
4. All of the forces are quite low and hence some strain readings - especially in the meridional direction - may be within the threshold of the data acquisition capability.
5. The maximum strain recorded corresponds to a concrete compressive stress of about 460 psi (3.2 MPa) hence structural failure must have been initiated by some mechanism other than by exceeding material limits.

In Fig.13 the support column loads obtained from the average of two sets of strain readings are plotted along with the straight line representing the theoretical load if the column carries 4/9 of the top cover load.This assumption appears to be reasonably correct and refinements were not made when computing shell membrane forces and buckling load.

Deflection profiles along vertical lines E and G are shown in Fig.14 for two intermediate loads. While these appear to show some significant lateral displacements the technique of data collection using the moveable dial support beam is suspect. More work will be done to standardize the procedure for moving and fastening the support beam to minimize shifts in zero readings.

The failed region of the shell is shown in Figs. 15-17. The hole occured between lines G and H at a load (vacuum) of 3.1 psi (446 psf or 21.4 kpa). Drawings of the appearance of the hole when viewed from outside the shell and inside are shown in Figs.16 and 17 respectively. The hole is

approximately elliptical in shape with major and minor diameters of about 16 in.(0.41 m) and 11.5 in.(0.29 m). The wire reinforcing had some concrete attached to it and was essentially straight.

This type of failure was not expected but is quite similar to those reported in Reference (23) for unreinforced concrete spherical caps.

In considering possible causes for this type of failure, the shell was again analyzed using Mungan's approach with the non-linear equations presented in Reference (14) but with an average thickness at the hole of 0.36 in. (9 mm) and a location of Z = 91 in.(2.3 m). Because of the assumption of non-linear material response it is necessary to calculate a critical load based on the membrane stress state at a given location for two cases - either the effect of N_ϕ predominates or else that of N_θ.

The consideration of non-linear material response assumes the uniaxial compressive stress-strain relation for concrete is satisfactorily represented by the Hognestad (Madrid) parabola. This is plotted in Fig.1 for the cylinder tested from concrete in lift 1. It is seen that good agreement is attained with the experimental curve for the micro-concrete.

As the results of these calculations which are presented in Table 6, show, the critical pressure is associated with N_ϕ but is only about 5% less than the value associated with N_θ.

These calculations were also made at locations where thicknesses were measured and the results again shown in Table 6. The calculated critical

load is in fact minimum at the location of the hole and again the effect of N_ϕ predominates slightly over N_θ. This is in light of the fact that N_ϕ is really considerable less than N_θ.

It is also noted that the wires will provide very little support in restraining the concrete because they are so far apart. Hence, this type of buckling must be quite similar to the unreinforced spherical dome. The suggestion that this mode of failure might occur has not been reported before.

Finally, it is seen that the actual pressure to cause buckling is about half that predicted using the method of Reference (14). The method described in Reference (16) using a grid analogy and using linear material response with $t = 0.5$ in.(13 mm) and $E_c = 3.8 \times 10^6$ psi (26.2 GPa) gave a buckling load of 3.2 psi(22 kPa).

CHAPTER VI

MERIDIONAL IMPERFECTION

In Reference (15), a general shape of imperfection is assumed, which becomes a straight line or a circular shape as two extremes depending on the value of a parameter 'C'.

Following Timoshenko, et al (22) and Reference (15), the hoop force and the meridional bending moment at the middle of the imperfection can be calculated, and are given below:

$$N_\theta = -n_\theta \, 2D_d \, K \, R \, N_\phi \, / \, H \quad \text{---------- (6-1)}$$

$$M_\phi = -m_\phi \, 2D_d \, N_\phi \, / \, H \, 2K \quad \text{----------(6-2)}$$

The tensile hoop force is positive, and the positive moment causes tension in the outer layer of the shell; n_θ and m_ϕ are the nondimensionalized hoop force and meridional moment coefficients, respectively. If the imperfection is of a circular shape, in the above equations:

$$n_\theta = 2 \, [1 - 2 \cos \bar{K} \exp(-\bar{K}) + \cos 2\bar{K} \exp(-2K)] \, / \, \bar{K} \quad \text{---- (6-3)}$$

$$m_\phi = 2 \, [2 \sin \bar{K} \exp(-\bar{K}) - \sin 2\bar{K} \exp(-2\bar{K})] \, / \, \bar{K} \quad \text{-----(6-4)}$$

For the straight line case of imperfection:

$$n_\theta = 1 - (\cos 2\bar{K} + \sin 2\bar{K}) \exp(-2\bar{K}) \quad \text{----------} \quad (6\text{-}5)$$

and

$$m_\phi = 1 - (\cos 2\bar{K} - \sin 2\bar{K}) \exp(-2\bar{K}) \quad \text{----------} \quad (6\text{-}6)$$

In which

$$\bar{K} = KH / 4$$

$$K^4 = 3 / R^2 t^2$$

H = length over which imperfection occures;

= distance between three measuring holes.

N_ϕ = tensile meridional force, based on membrane theory, in the shell subjected to uniform external pressure and 5/9 of vertical load on plate at top of shell.

R = radius of the shell

t = thickness of the shell

D_d = imperfection out of round from the perfect shape in the radial direction. The term D_d was discussed in chapter V with more detail.

A computer frogram was written to analyze stress and strain of this shell model due to uniform external pressure, vertical load on the plate at the top of shell and imperfections. The objective was to compare the strain of this shell collected by experiment with that based on theory. The electrical strain gage can not sense the strain due to dead load to which the shell has been subjected before the strain gage was mounted, so, the stresses due to dead load are not included in the computer program.

The results of the computer caculation and experiment data are drawn in Fig. 8 - 12. The processes will be shown in Appendix III. The agreement between the experiment data and the computer caculation was good in the circumferential direction. But, in the meridional direction, the agreement was not satisfied. The outside strain at throat of line E, base of line H and inside strain at four feet below throat of line H went to positive. Hence, the structural response is unsymmetrical even with symmetrical load. It may occur due to imperfection of geometry and thickness.

CHAPTER VII

CONCLUSIONS

The failed hole occured between line G and H. The center of the hole was 16 in.(41 cm) above the bottom. According to the computer analysis the strain there was not the largest. The failure may be just local, but it is quite similar to those reported by Vandepitte and Rathe (23) for spherical concrete shells.

The geometry and thickness imperfections produce additional stresses and moments which may cause local failure. To control the geometry imperfection in this shell model a level and plumb were used. It is relatively easier to control the geometry than the thickness. Fiber-glass was used to make the formwork. Its advantage is that it is easy to fabricate and light in weight, but, the stiffness is not good enough. The thickness was difficult to control because the curvature was changed everywhere in both meridion and circumference direction. Perhaps, one can surface the inner form, give up the outer form and use sprayed concrete.

The experimental data for the strain in the circumferential direction was quite close to the membrane theory when the effects of meridional imperfection were considered. Although the agreement for the meridional direction strains was not so good as that for the circumferencial direction, the experimental data is valuable. The work presented herein should provide useful data for additional analytical studies. However, direct similitude extrapolation to prototype shells is not possible.

It is also seen that the failure pressure, 3.1 psi (21 kPa), is about half the predicted buckling pressure using the method of Reference (14). The method described in Reference (16) using a grid analogy and using linear material gave a buckling load of 3.2 psi (22 kPa). So, by considering the model as a prototype useful conclusions regarding current methods for predicting shell forces and buckling response can be made.

References

1. Abel, J.F., and Billington, D.P., "Stability Analysis of Cooling Towers: A Review of Current Methods." "Shell Structures and Climatic Influences," Proceedings of the International Association for Shell Structures Symposium, University of Calgary, Calgary, Alberta, Canada, July, 1972.

2. Abel, J.F., Billington, D.P., Nagy, D.A., and Wiita-Dworkin, C., "Buckling of Cooling Towers." Research Report No. 79-SM-1, Department of Civil Engineering, Princeton University, Princeton N.J., January 1979.

3. Abel, J.F., and Gould, P.L., "Buckling of Concrete Cooling Tower Shells." ACI Publication SP-67 "Concrete Shell Buckling," 1981.

4. ACI-ASCE Committee 334, "Reinforced Concrete Cooling Tower Shell - Practice and Commemtary," Journal of the ACI, Vol.74, January 1977.

5. Billington, D.P., "The Buckling of Concrete Cooling-Tower Shells," Proceedings of the Pacific Symposium on Hydromechanically Loaded Shells, International Association for Shell Structures, Oct. 1971.

6. Billington,D.P., and Harris, H.G., "Test Methods for Concrete Shell Buckling," ACI Publication SP-67, "Concrete Shell Buckling," 1981.

7. Bushnell, D., "Stress, Stability, and Vibration of Complex Branched Shells of Revolution: Analysis and User's Manual for BOSOR 4," Report LMSC-D243605, National Aeronautics and Space Administration/Langley Research Center, Hampton, Va., March 1972.

8. Cole, P.P., Abel J.F., and Billington, D.P., "Buckling of Cooling Tower Shells: State-of-the-Art," Journal of the Structural Devision, ASCE, Vol. 101, No.ST6, Proc. Paper 11364, June 1975.

9. Cole, P.P., Abel J.F., and Billington, D.P., "Buckling of Cooling Tower Shells: Bifurcation Results," Journal of the Structural Division, ASCE, Vol.101, No ST6 Proc. Paper 11365, June, 1975.

10. Croll, J.G.A., Kaleli, F., and Kemp, K., "Meridionally Imperfect Cooling Towers," Journal of the Engineering Mechanics Division, ASCE, Vol. 105, No.EM5, Oct. 1979.

11. Croll, J.G.A., and Chilver, A.H., "Apporximate Estimates of the Stability of cooling Towers under Wind Loading," Proceedings, International Association for Shell Structures Colloquium on Recommendations for the Structural Design of Hyperbolic or Other Similarly Shaped Cooling Towers, Brussels, Belgium, May, 1971.

12. Croll, J.G.A., and Kemp, K.O., "Specifying Tolerance Limits for Meridional Imperfections in Cooling Towers," Journal of the American Concrete Institute, January 1979.

13. Der, T.J., and Fidler, R., "A Model Study of the Buckling Behavior of Hyperbolic Shells," Proceedings, Institution of Civil Engineers, Vol. 41, London, England, Sept., 1968.

14. Gates, T.E., Hu, K.K., McDonald, C.R. and Swartz, S.E., "Construction and Testing of Micro-Concrete Models of Cooling-Tower Shells," Proceedings, Fourth International Congress on Experimental Mechanics, Society for Experimental Stress Analysis, 1981.

15. Gupta, A.K., and Al-Dabbagh, A., "Meridional Imperfection in Cooling Tower Design - Update". Presented at the ASCE International Convention, New York, N.Y. May, 1981.

16. Hu, K.K., Kirmser, P.G., Swartz, S.E., and Pan, C., "On the Matrix Analysis of Non-Linear Buckling of Hyperbolic Cooling Towers," Presented at the Joint ASME/ASCE Mechanics Conference, Boulder, CO. June 22-24, 1981.

17. Krätzig, W.B., and Zerna, W., "Resistance of Hyperbolic Cooling Towers to Wind and Earthquake Loading," Structural Engineering and Structural Mechanics by Karl S. Pister, Editor, 1980.

18. McDonald, C.R., and Swartz, S.E., "Use of Strain Gages on Miniature Concrete Cylingers," Experimental Techniques, Vol.5, No.1, Mar. 1981.

19. Mungan, I., "Buckling Stress States of Hyperboloidal Shells", Journal of the Structural Division, ASCE, Vol.102, No. ST10, Proc. Paper 12465, October, 1976.

20. Schnobrich, W.C., "Analytical and Numerical Evaluation of the Buckling Strength of Reinforced Concrete Shells," ACI Publication SP-67 "Concrete Shell Buckling", 1981.

21. Swartz, S.E., "Buckling Behavior of Concrete Shells," Annual Report to the National Science Fundation for the period June 1, 1979 to May,31, 1980.

22. Timoshenko, S. and Woinowsky - Krieger, S., "Theory of Plates and Shells" McGraw-Hill Book Co., Inc., New York, NY. 1959.

23. Vandepitte, D., and Rathe, J., "An Experimental Investigation of the Buckling Load of Spherical Concrete Shells, Subjected to Uniform Radial Pressure, "RILEM International Symposium, Buenos Aires, Argentina, Sept. 13-18, 1971.

Appendix I : Tables

Table 1. Properties of Micro-Concrete and Reinforcing

Micro - Concrete

Sieve Analysis of Kaw River

Sand - Percent Retained:

No. 16 = 0
No. 30 = 17
No. 50 = 78
No. 100 = 98
No. 200 = 99

Fineness Modulus = 2.92

Steel Wire

Diameter = 0.105 in.(2.7 mm)

Avg. yield stress = 81.9ksi(564MPa)

Avg. modulus of elasticity, E_s = 29.8 X 10^6 psi (206 GPa)

40 wires per ruling direction evenly spaced (80 wires total) nominal steel ratio = 0.35%

Quantities Per Cu. Ft. Mix:

Cement (Type I)	38.46 lb (171.1N)
Sand	76.92 lb (342.3N)
Water	19.23 lb (85.6N)
HEC 400*	0.069 lb (0.31N)
Set Retarder	25 ml
Air	2%
Unit Weight	135 lb/cu. ft. (21.2 kN/m^3)
Slump	4 in.

Properties of hardened mix: using 3 in.X 6 in.(76 mm X 152 mm) cylinders tested at age 95 days or older

Avg.

f_c'= 6280 psi (43.3 MPa)

ε_o = 3.58 X 10^{-3} in./in. (m/m)

E_c = 3.62 X 10^6 psi (24.9 Gpa)

Split cylinder tensile strength = 660 psi (4.5 MPa)

Poisson's Ratio = 0.16

*Set retarder - used in first lift only.

Table 2. Cylinder Test Log, Shell No. 1

	Casting Date	Testing Date	Compressive Strength f_c psi (MPa)	Age at Test days (Ms)
	10 April 81	17 April 81	5130 (35.3)	7 (0.6)
	10 April 81	17 April 81	4810 (33.1)	7 (0.6)
	10 April 81	24 April 81	5870 (40.4)	14 (1.2)
	10 April 81	24 April 81	4900 (34.4)	14 (1.2)
	17 April 81	24 April 81	3990 (27.5)	7 (0.6)
	17 April 81	24 April 81	3540 (24.4)	7 (0.6)
	27 April 81	4 May 81	3850 (26.5)	7 (0.6)
	27 April 81	4 May 81	3850 (26.5)	7 (0.6)
	17 April 81	4 May 81	4780 (32.9)	17 (1.5)
	17 April 81	4 May 81	4340 (29.9)	17 (1.5)
	10 April 81	31 July 81	4240 (29.2)	112 (9.7)
	27 April 81	31 July 81	+ 5560 (38.3)	95 (8.2)
*	17 April 81	31 July 81	+ 5940 (40.9)	105 (9.1)
	17 April 81	17 Nov. 81	^ 6270 (43.2)	214 (18.5)
	27 April 81	17 Nov. 81	^ 5720 (39.4)	204 (17.6)
*	10 April 81	17 Nov. 81	^ 6850 (47.2)	221 (19.1)

* cylinder stress-strain data obtained and plotted in Fig. 1

+ Average value is 5750 psi (39.6 MPa)

^ Average value is 6280 psi (43.3 MPa)

Note: All cylinders 3 in. X 6 in. (76 mm X 152 mm) and were cured in ambient conditions adjacent to the shell.

Table 3, Deviation From Ideal Geometry

Shell No. 1

Merid. Location		Theo. Radius r, in.	Deviations, inches (horizontal component) A	B	C	D	E	F	G	H	I	J	K	L	Dist. From Throat Z, in.
Lift 3	1	38.4	-.21	+.15	+.42	+.20	-.13	-.41	-.93	-.19	-.06	-.22	-.63	-.47	- 33
	2	37.24	-.12	+.12	+.55	+.58	+.07	-.42	-.84	+.06	-.09	-.19	-.68	-.50	- 24
	3	36.31	-.54	+.03	+.61	+.53	+.09	-.68	-.81	-.01	+.04	-.36	-.86	-.77	- 12
	4	36.00	-.83	-.16	+.67	+.62	+.19	-.80	-.88	+.13	+.20	-.61	-.81	-1.01	0
Lift 2	5	36.31	-.86	+.05	+.74	+1.02	+.45	-.54	-.62	+.45	+.73	-.29	-.46	-.84	+ 12
	6	37.24	-.70	+.05	+.74	+.91	+.45	-.64	-.47	+.31	+.78	-.08	-.34	-.89	+ 24
	7	38.74	-.64	+.19	+.80	+1.12	+.73	-.39	-.21	+.58	+.80	+.32	-.15	-.68	+ 36
	8	40.74	-1.14	-.17	+.39	+.60	+.48	-.68	-.45	+.14	+.20	+.10	-.45	-.92	+ 48
Lift 1	9	43.17	-.53	-.18	+.18	+.81	+.51	-.57	-.18	+.13	+.70	+.46	+.05	-.28	+ 60
	10	45.98	-.25	-.66	-.82	+.98	+.46	-.40	-.32	+.05	+.39	+.66	-.20	+.12	+ 72
	11	49.08	-.74	-1.56	-1.15	+.09	+.69	-.41	-.14	-.03	+.56	+.57	+.26	-.01	+ 84
Max. Deviation in 24 in., S%			-4.6	2.1	3.3	4.4	2.2	-2.7	-2.1	3.0	-4.6	2.6	3.1	-3.7	

(-) = outward (+) = inward 1 in. = 25.4mm

Table 4. Shell Thicknesses - Shell No. 1

	Merid. Location	Thickness, inches												Dist. From Throat Z, in.
		A	B	C	D	E	F	G	H	I	J	K	L	
Lift 3	1	0.41	1.02	0.37	0.56	0.71	0.48	0.45	0.58	0.72	0.51	0.25	0.68	- 33
	2	0.25	0.75	0.61	0.32	0.61	0.43	0.31	0.41	0.74	0.48	0.29	0.18	- 24
	3	0.61	0.54	0.42	0.75	0.97	0.58	0.79	0.78	0.85	0.58	0.58	0.73	- 12
	4	0.60	0.52	0.33	0.76	0.41	0.64	0.46	0.49	0.65	0.61	0.57	0.59	0
Lift 2	5	0.72	0.47	0.38	0.65	0.54	0.65	0.61	0.32	0.59	0.42	0.49	0.69	12
	6	0.41	0.40	0.31	0.96	0.75	0.89	0.67	0.61	0.62	0.51	0.32	0.78	24
	7	0.33	0.61	0.42	0.72	0.86	0.81	0.42	0.62	0.65	0.36	0.51	0.73	36
	8	1.45	1.11	1.15	1.07	1.24	0.85	0.78	1.44	1.45	0.58	1.61	1.28	48
Lift 1	9	0.83	1.27	1.27	0.87	1.05	1.10	0.73	1.45	0.57	0.68	0.95	0.60	60
	10	0.75	2.21	2.57	0.44	0.97	1.07	1.35	1.48	0.79	0.65	0.86	0.81	72
	11	1.07	3.30	2.70	0.91	0.72	1.28	1.31	1.81	0.78	0.52	0.68	1.01	84

1 in. = 25.4mm

Table 5. Experimental Bending Moments and Forces at Maximum Load, Shell No. 1

Location	M_ϕ lb - in/in (N - m/m)	M_θ lb - in/in (N - m/m)	N_ϕ lb - in/in (kN/m)	N_θ lb - in/in (kN/m)
Top of shell just below ring on Line H	44 (196)	2 (9)	53 (9)	35 (6)
Throat, Line H	-2.8 (-12.5)	-8.5 (-38)	-50 (-9)	-93 (-16)
Four feet below throat, Line H	2.4 (10.5)	-113 (-503)	10 (2)	-109 (-19)
Base, Line H	-63 (-280)	-67 (-298)	-65 (-11)	-133 (-23)
Throat, Line E	-2.4 (-10.7)	10 (44)	-33 (-6)	-234 (-41)
Throat, Line B	5.3 (23.6)	20.6 (92)	-94 (-16)	-201 (-35)

Poisson's Ratio is 0.16

Tensile hoop force is positive and the positive moment causes tension in the outer layer of the shell.

Table 6. Predicted Pressures and Internal Forces

Associated With Possible Local Buckling, Shell No, 1

Location	Vertical Distance Z in. (m)	Shell Thickness h in. (mm)	Buckling Pressure, q_{cr} based on N_ϕ psi (kPa)	Buckling Pressure, q_{cr} based on N_θ psi (kPa)	Membrane Forces using q_{cr} based on N_ϕ: N_ϕ lb/in (kN/m)	Membrane Forces using q_{cr} based on N_ϕ: N_θ lb/in (kN/m)
Hole	91 (2.31)	0.36 (9)	6.53 (45)	6.90 (48)	-128 (-22)	-355 (-62)
Line A	36 (0.91)	0.33 (8)	7.19 (50)	7.60 (52)	-77 (-13)	-292 (-51)
Line C	24 (0.61)	0.31 (8)	6.54 (45)	6.90 (48)	-62 (-11)	-254 (-44)
Line H	12 (0.30)	0.32 (8)	7.24 (50)	7.65 (53)	-64 (-11)	-273 (-48)

Notes: 1. Buckling pressure calculated using equations of Reference 1 and f'_c = 6280 psi (43.3 MPa), εo = 0.00358 in/in (m/m), Poisson's Ratio = 0.16, Unit weight = 135 lb/ft^3 (21.2 kN/m^3).

2. The value of q_{cr} given in Reference 2 for h = 0.5 in. (13mm) is 3.2 psi (22 kPa) and the actual failure pressure was q_F = 3.1 psi (21 kPa).

Appendix II : Figures

THIS BOOK CONTAINS NUMEROUS PAGES WITH DIAGRAMS THAT ARE CROOKED COMPARED TO THE REST OF THE INFORMATION ON THE PAGE.

THIS IS AS RECEIVED FROM CUSTOMER.

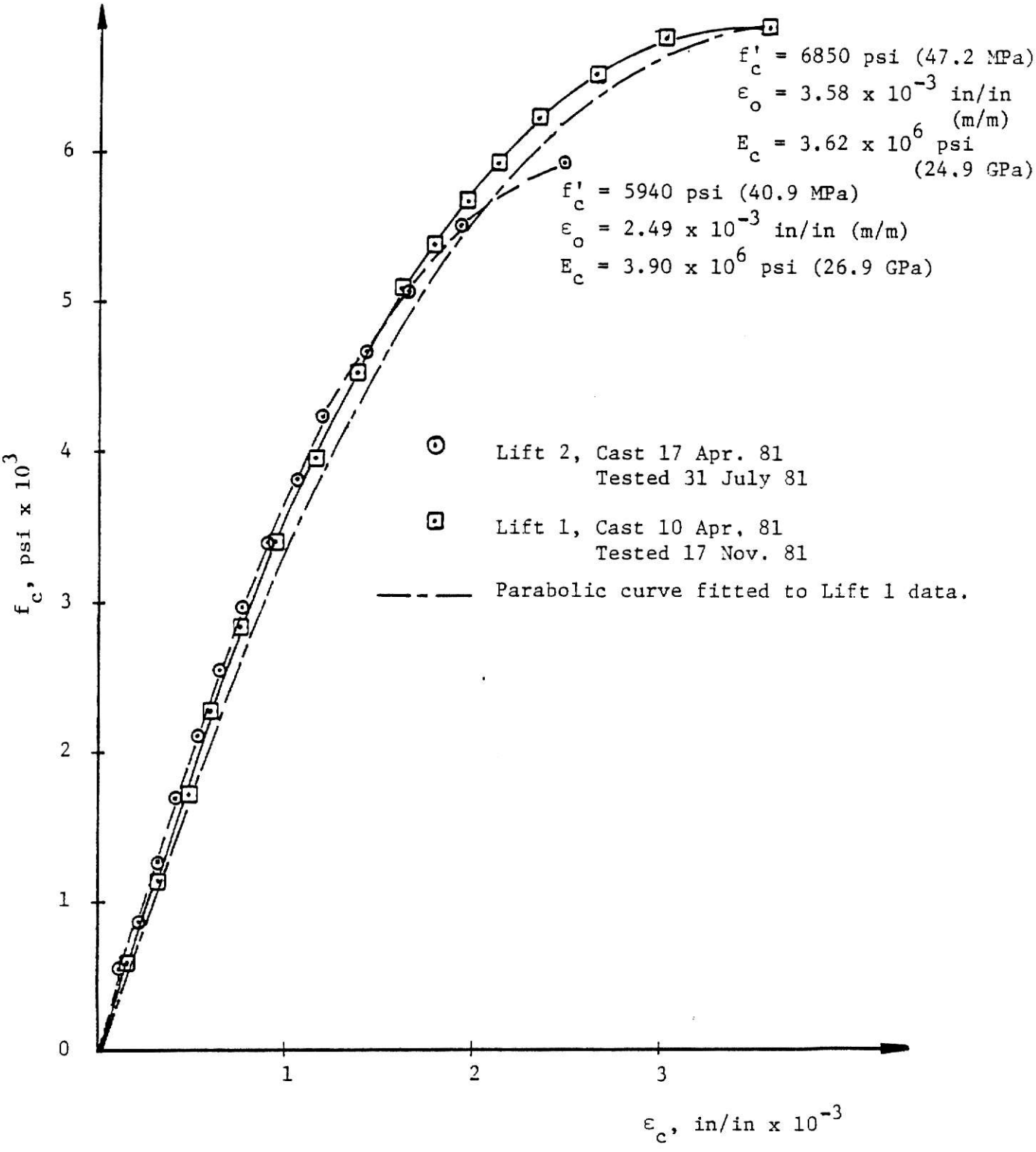

Fig. 1. Cylinder Tests, Shell No. 1

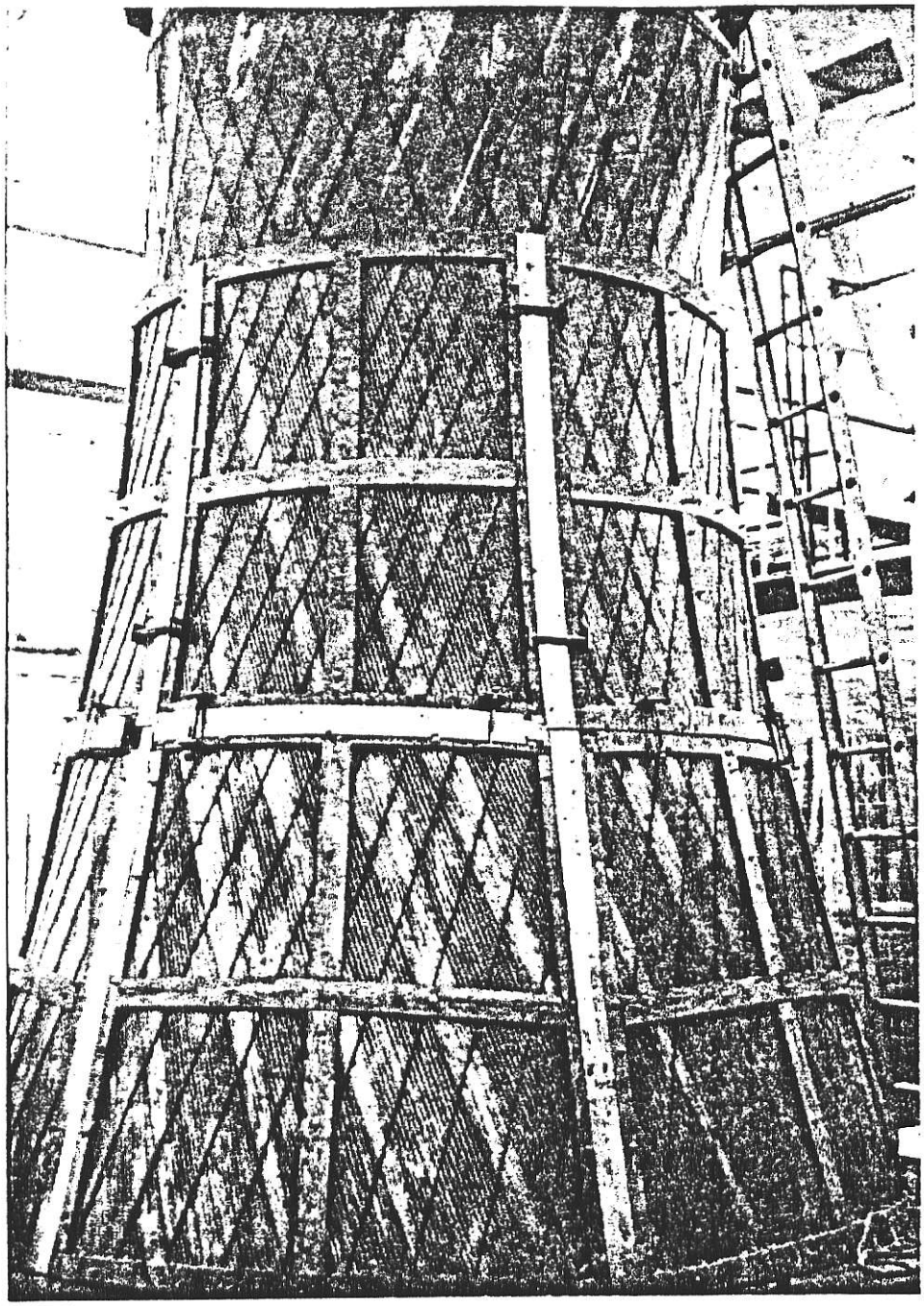

Fig. 2 Formwork, Shell No. 1

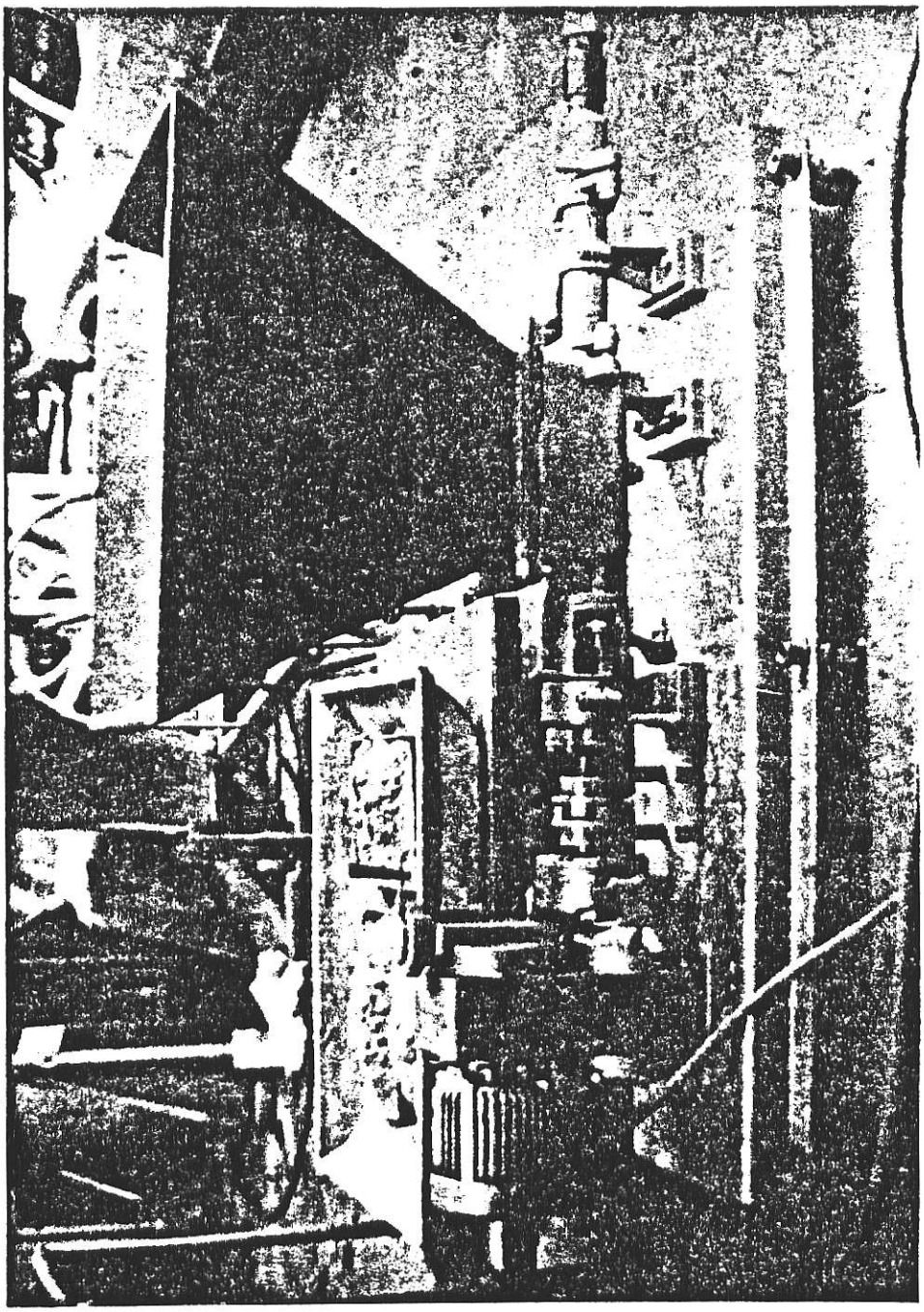

Fig. 3 Concrete Pump

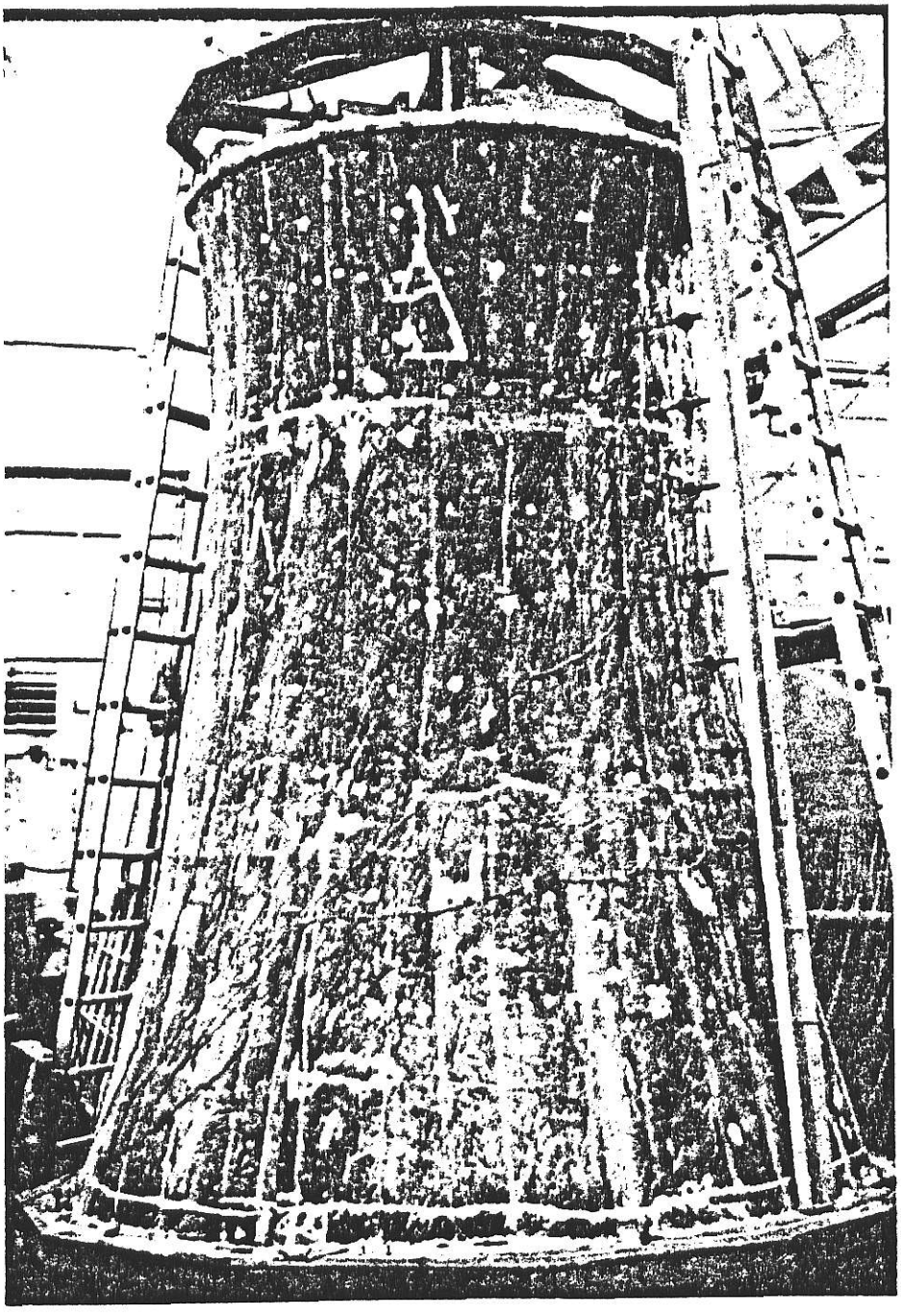

Fig. 4 Shell No. 1 With Deflection Gage Support Beam

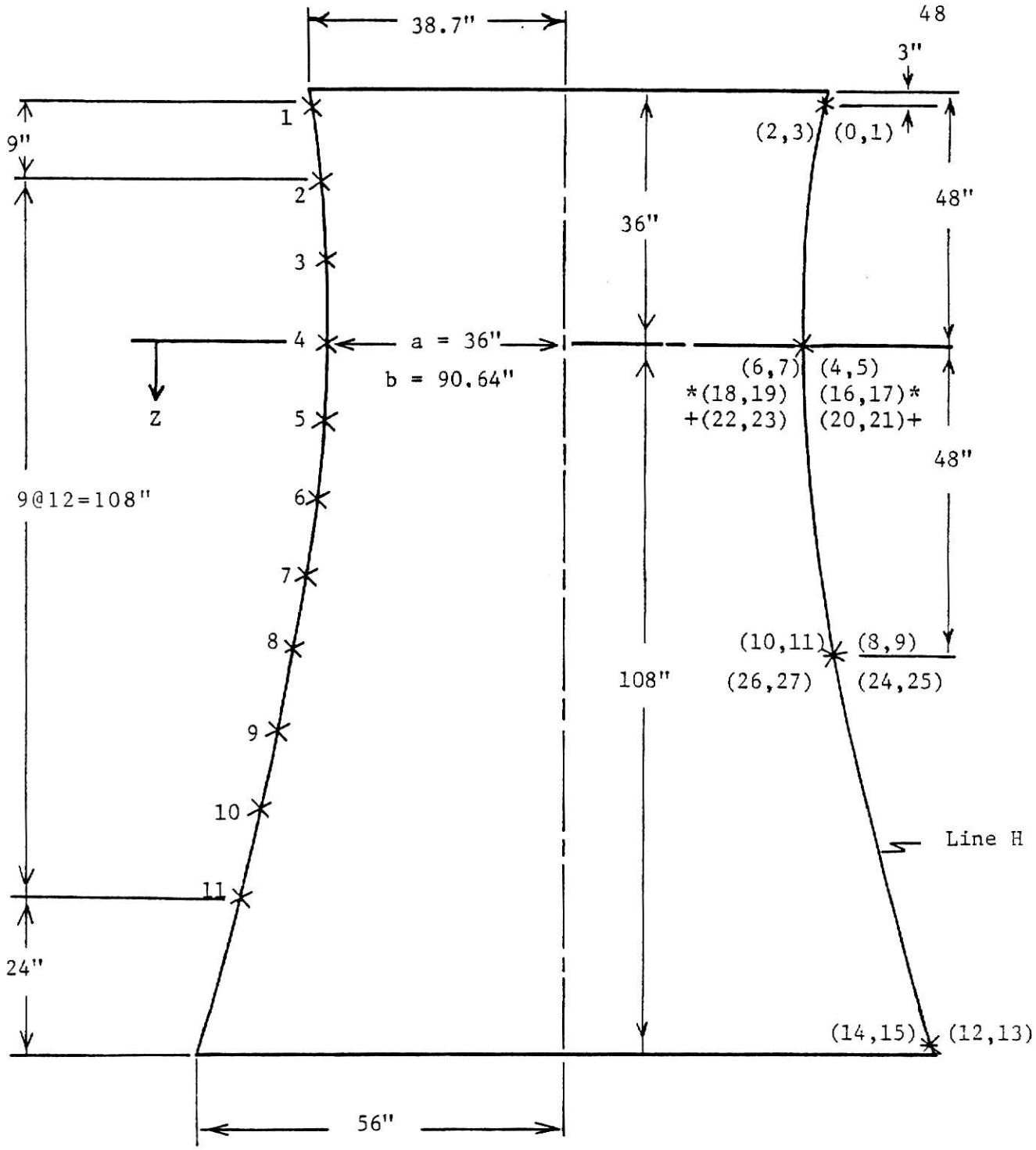

* Throat, Line E + Throat, Line B

⋇ Locations for thickness, geometry, displacement data

( ) = two-element rosettes, even-circumferential; odd-meridional

Refer to Fig. 6 for circumferential locations 1 in. = 0.0254m

Fig. 5. Meridional Locations for Thickness, Geometry Displacement and Strain Data

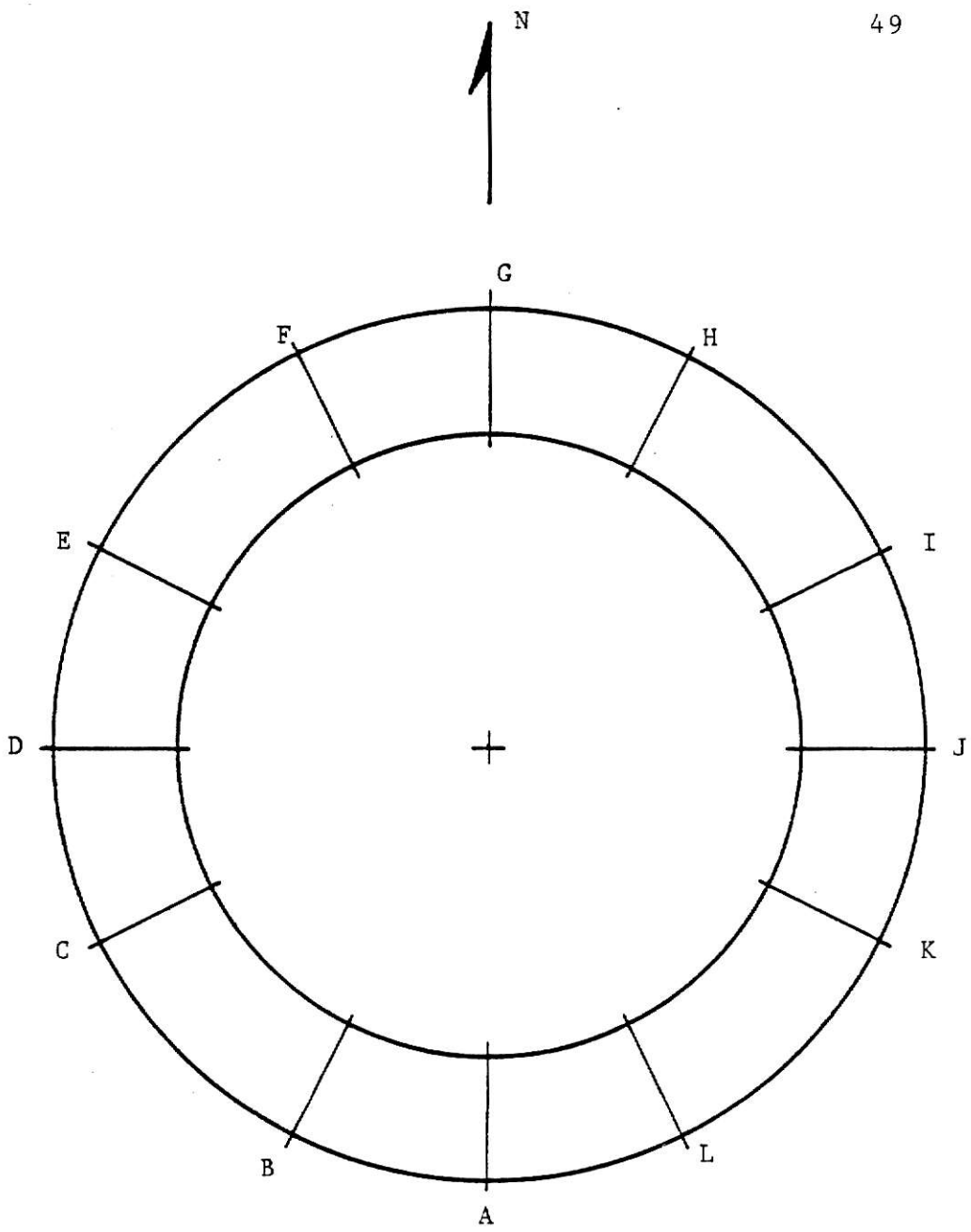

Refer to Fig. 5 for meridional locations.

Fig. 6. Circumferential Locations For Thickness, Geometry and Displacement Data, Shell No. 1

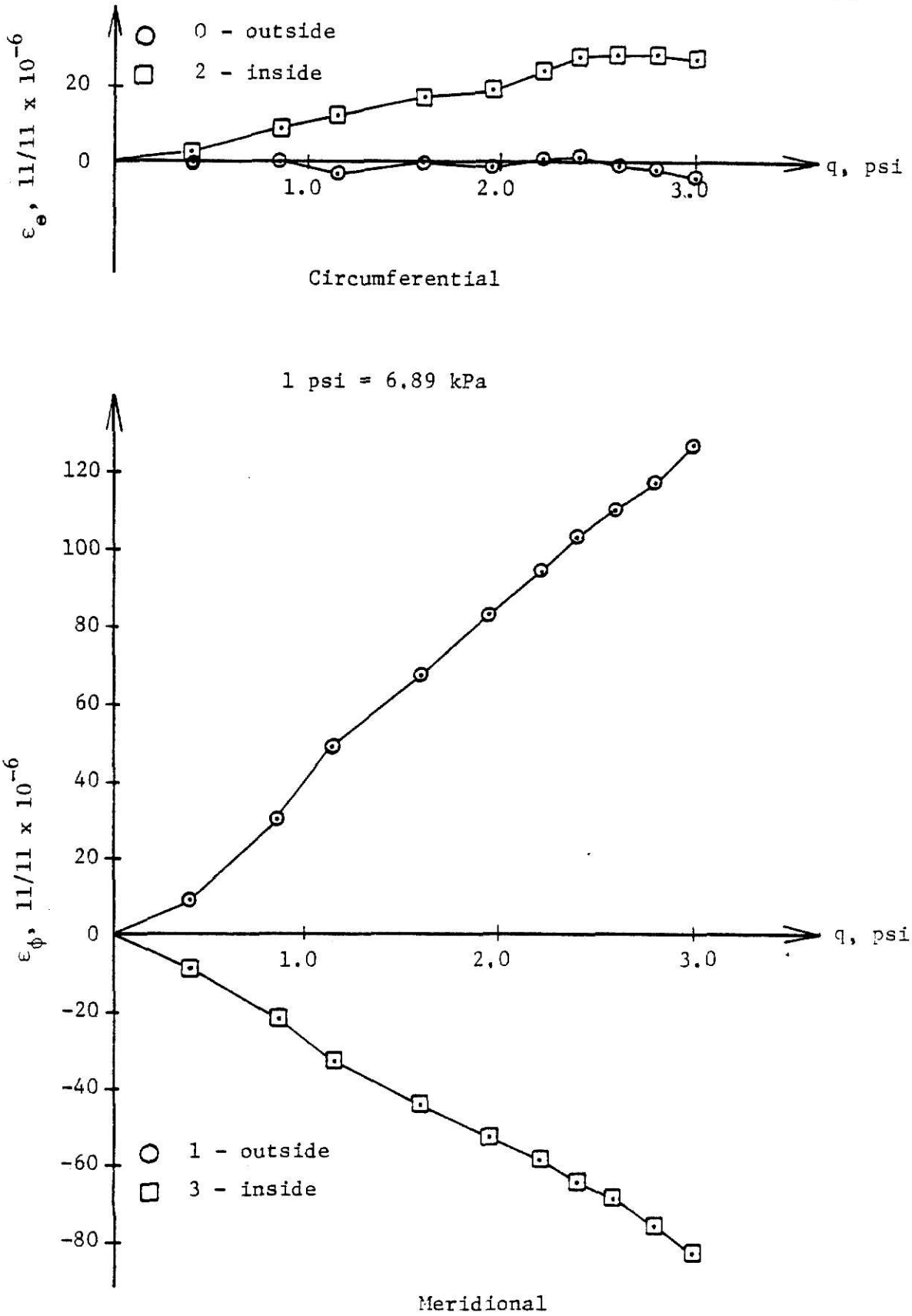

Fig. 7. Strain at Top of Shell Just Below Ring, Line H, Shell No. 1

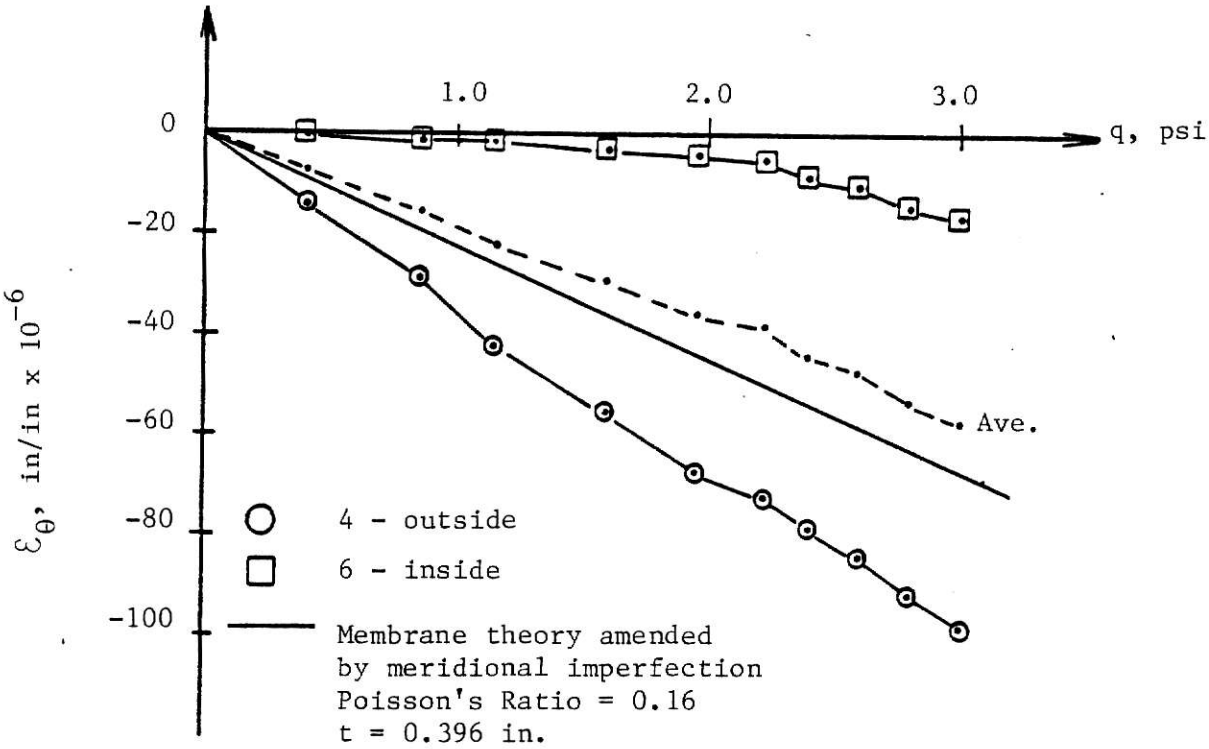

Circumferential

1 psi = 6.89 kPa

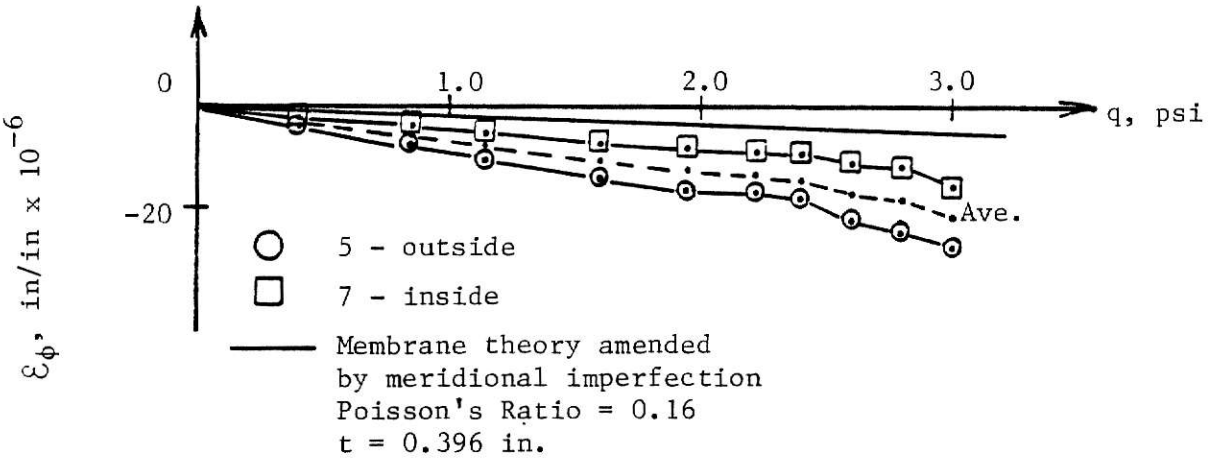

Meridional

Fig. 8. Strain at Throat, Line H, Shell No.1

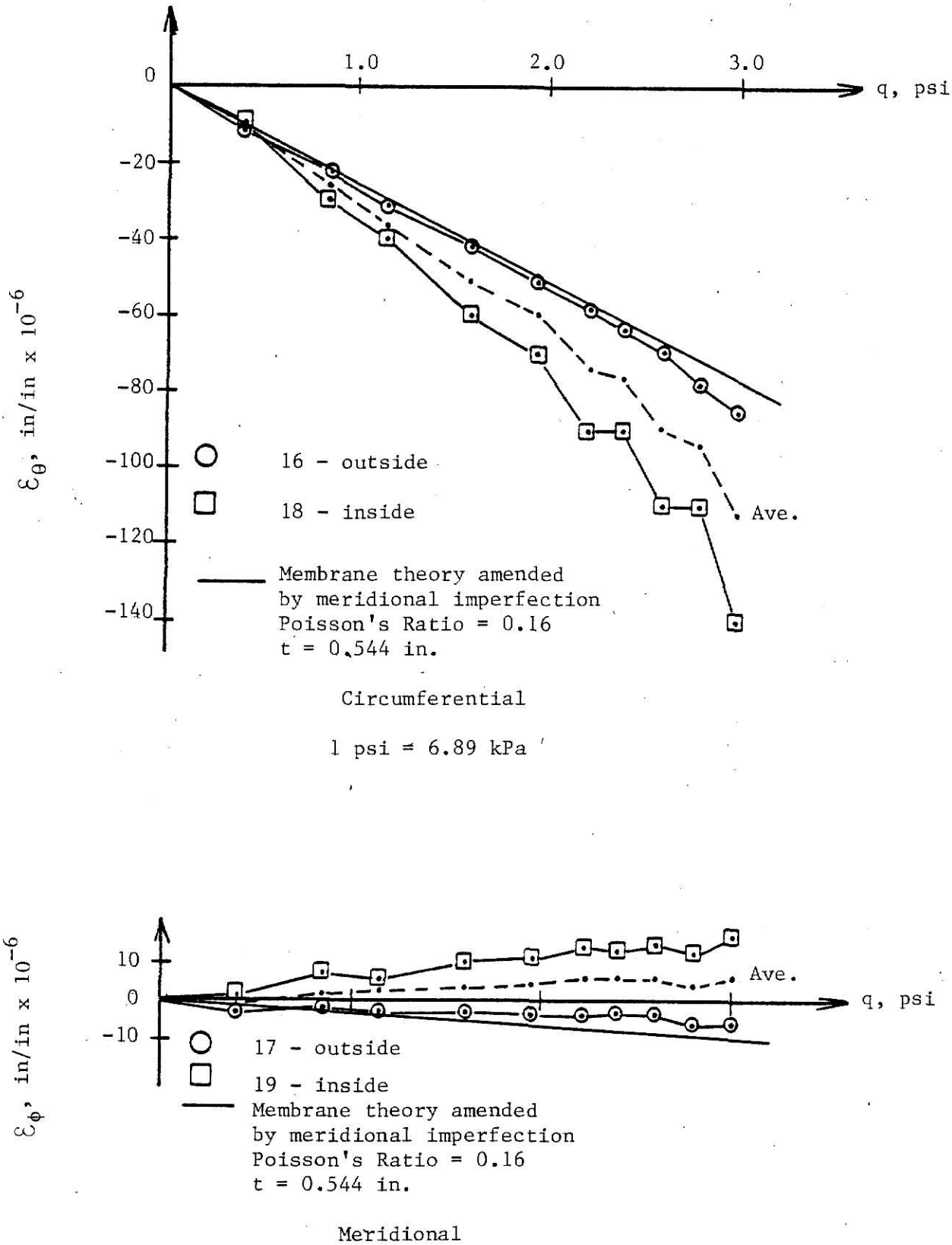

Fig. 9. Strain at Throat, Line E, Shell No. 1

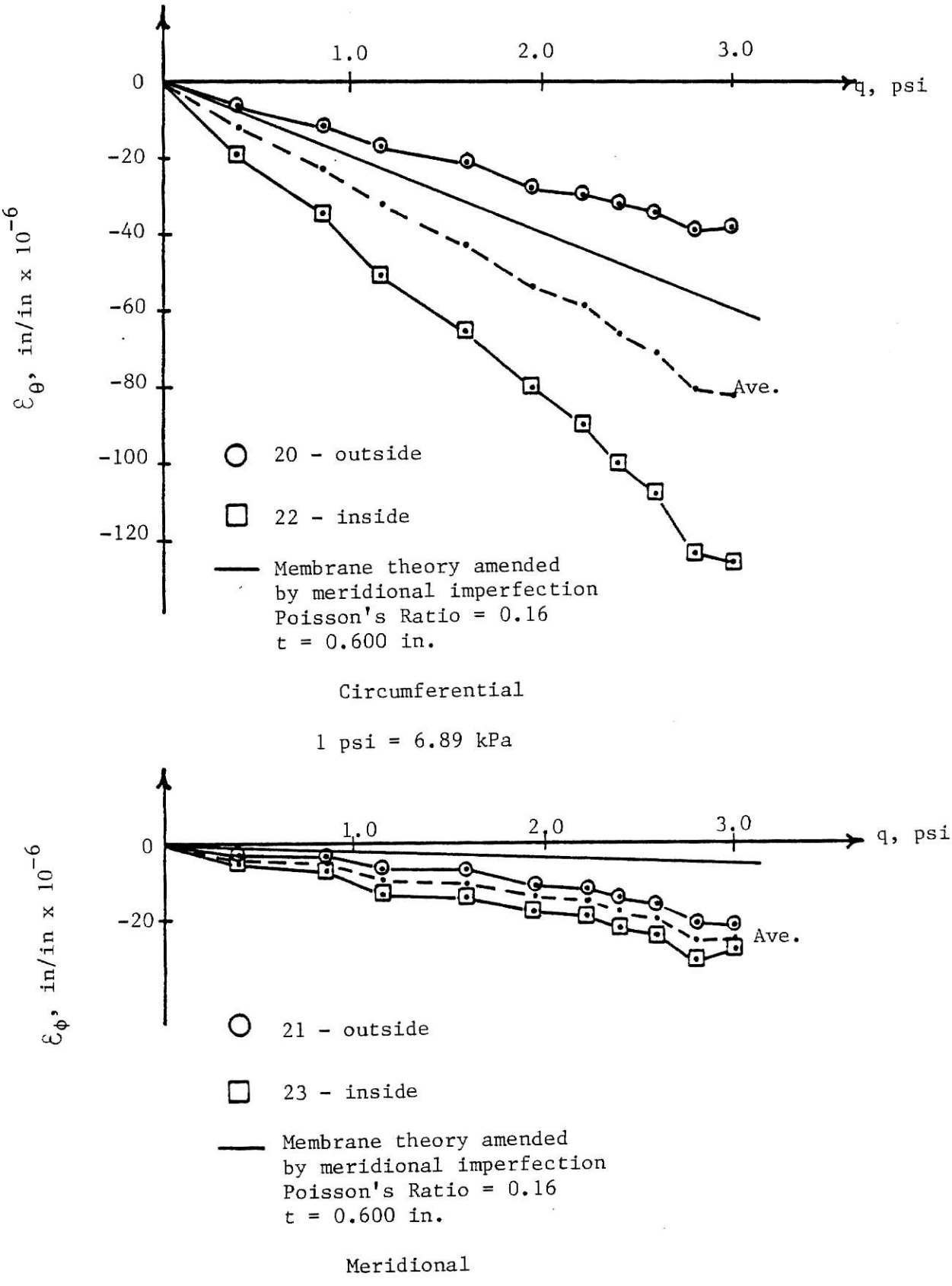

Fig. 10 Strain at Throat, Line B, Shell No. 1

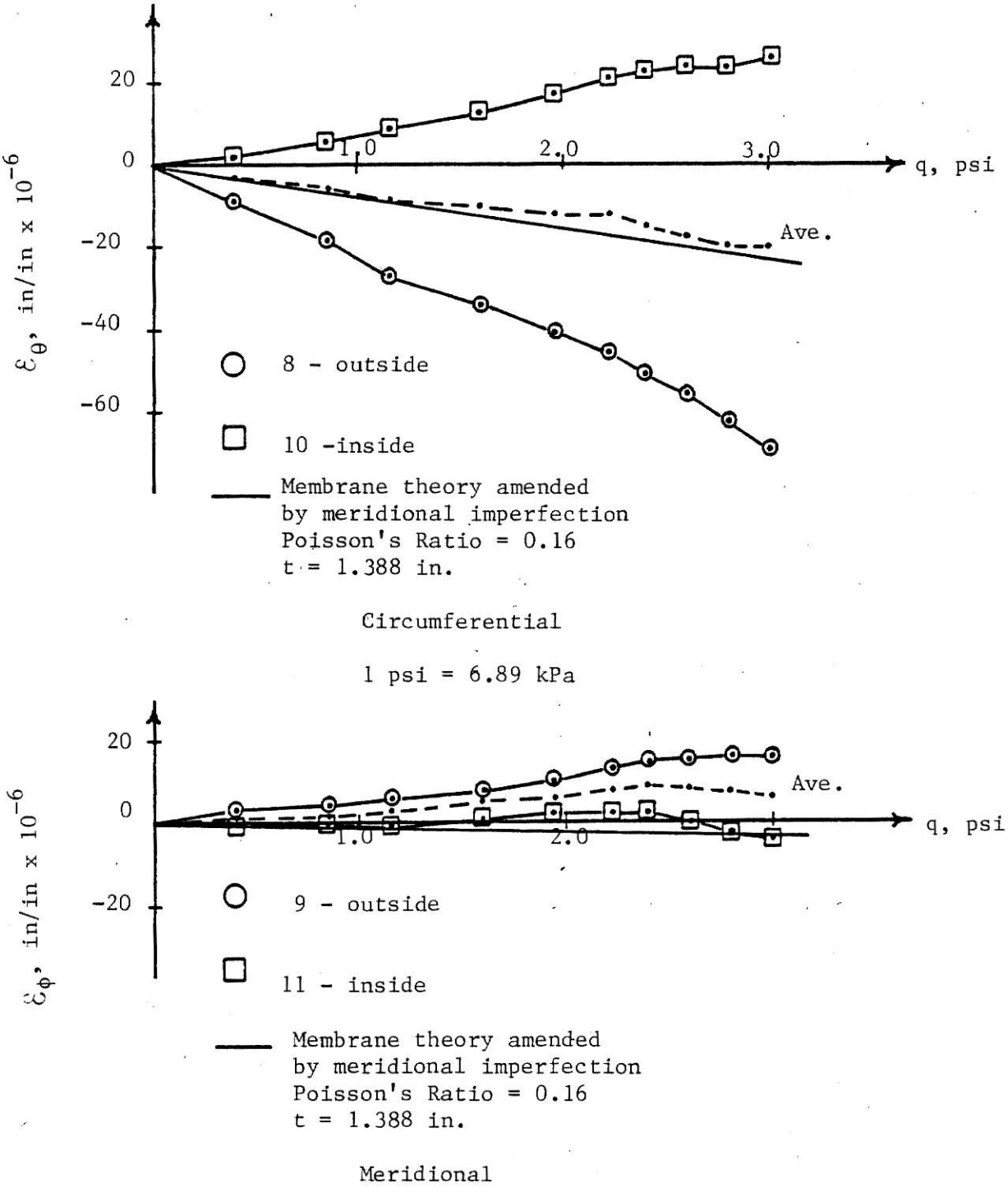

Fig. 11. Strain Four Feet Below Throat, Line H, Shell No. 1

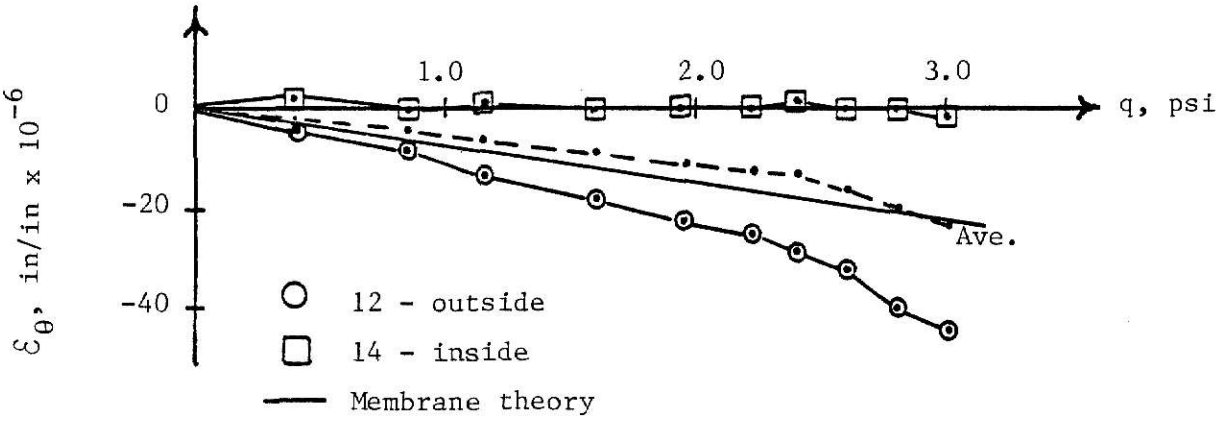

Poisson's Ratio = 0.16
t = 1.44 in.

Circumferential

1 psi = 6.89 kPa

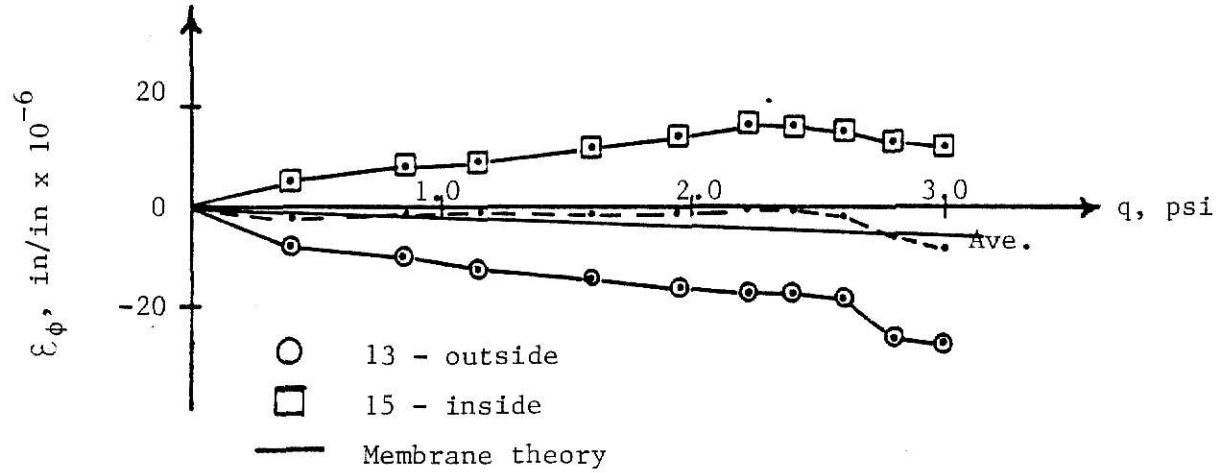

Poisson's Ratio = 0.16
t = 1.44 in.

Meridional

Fig. 12. Strain at Base, Line H, Shell No. 1

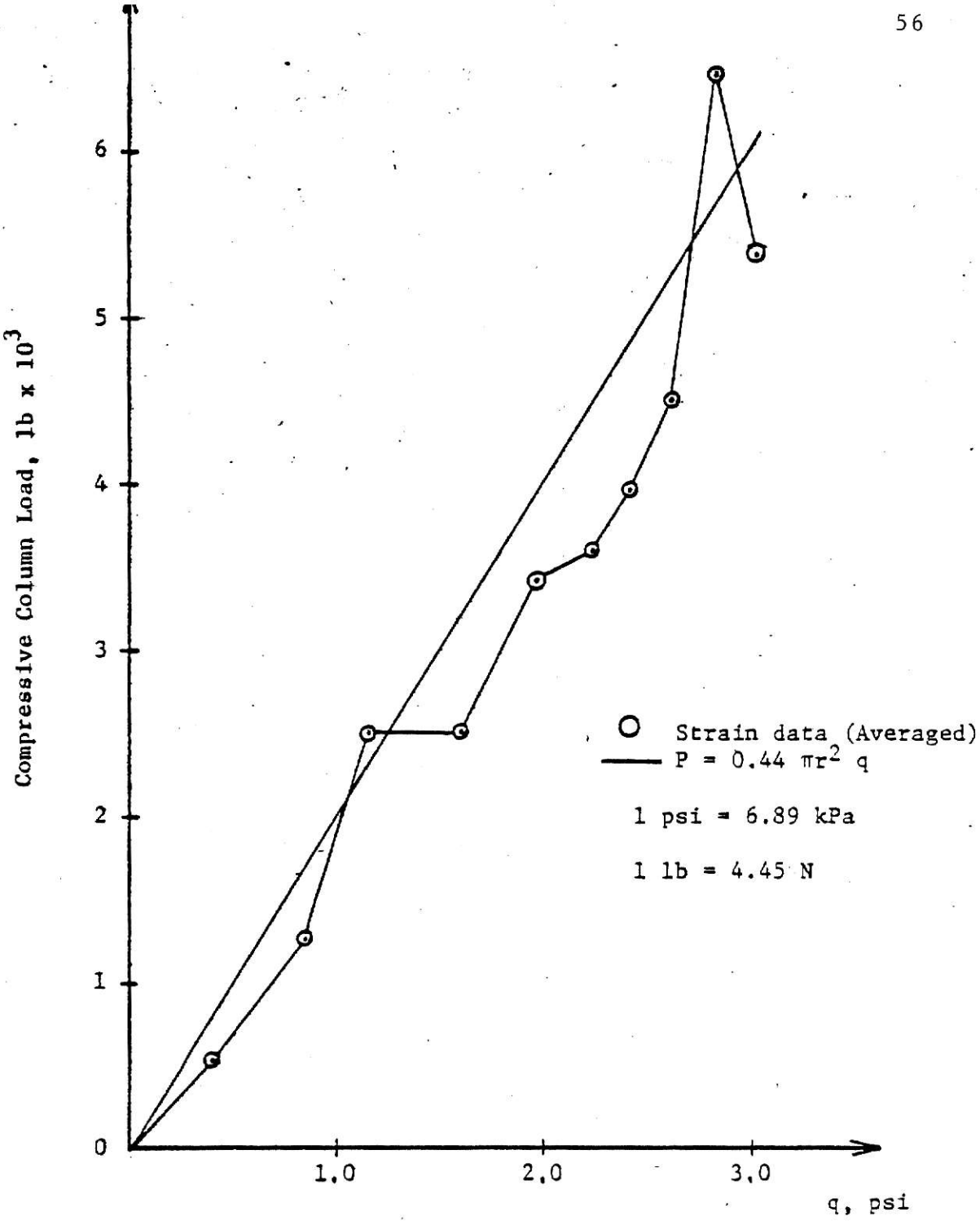

Fig. 13. Measured and Theoretical Support Column Loads

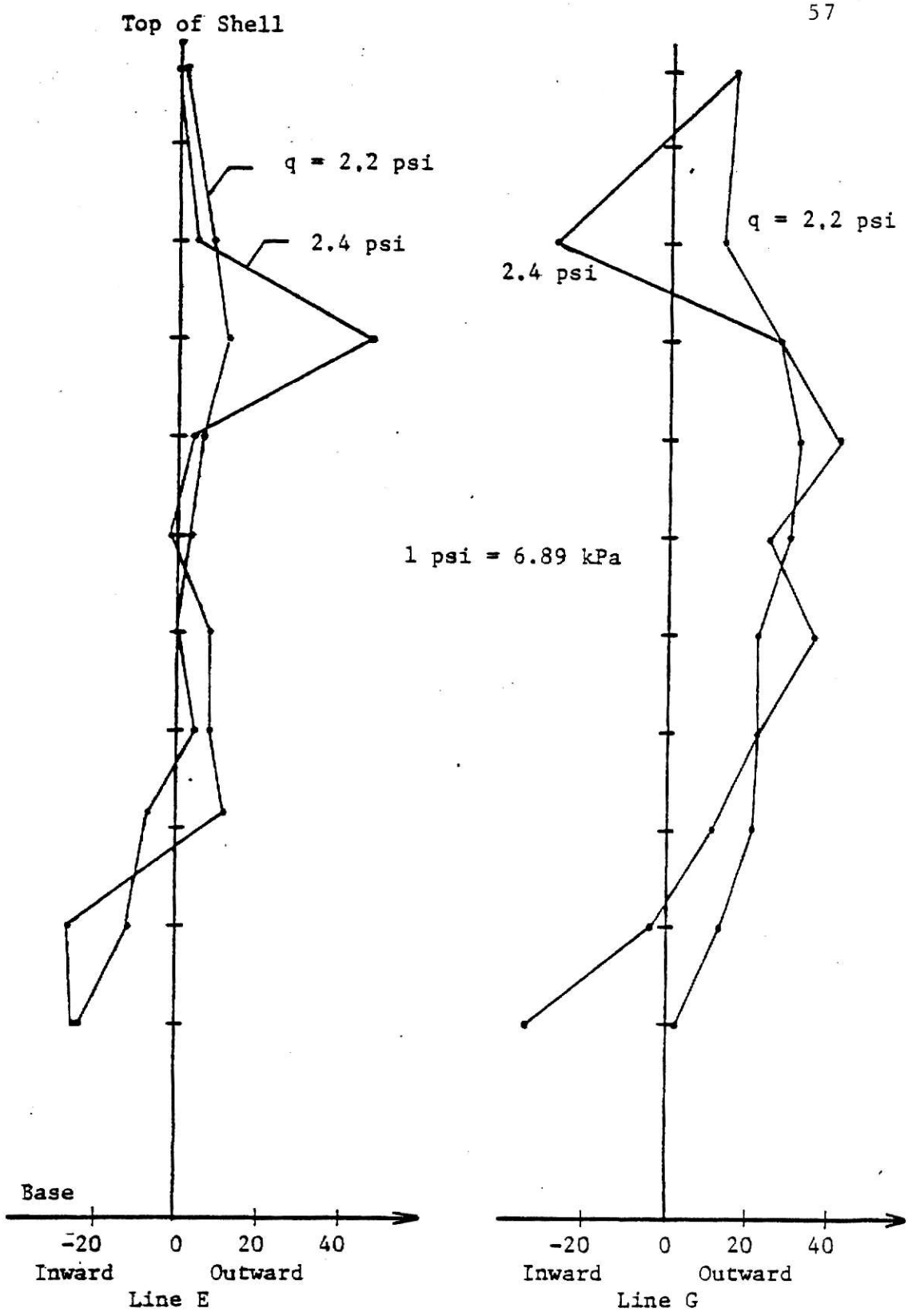

Deflections, in x 10^{-3} , 1 in. = 25.4mm

Fig. 14. Deflection Profiles

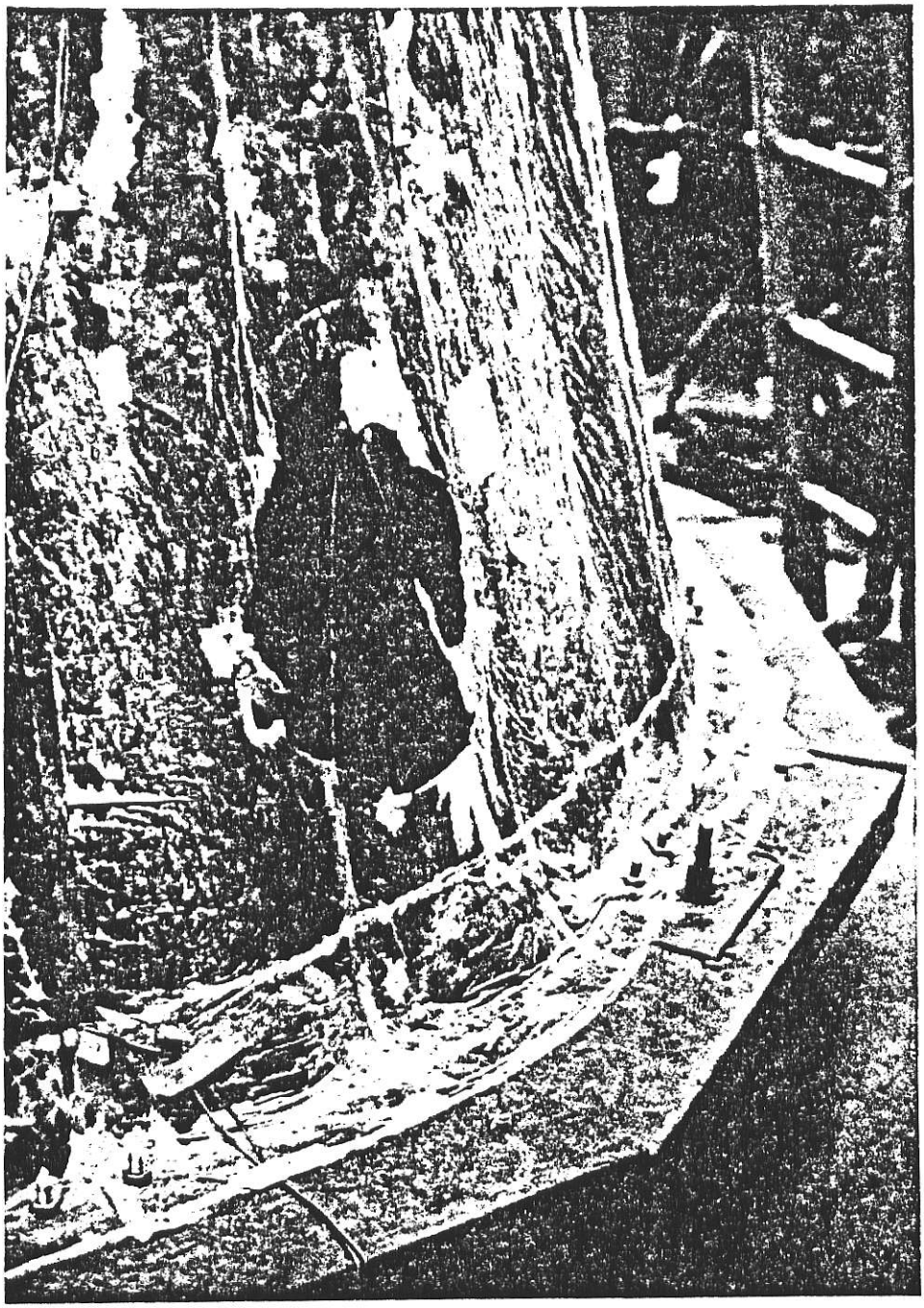

Fig. 15 Failed Region, Shell No. 1

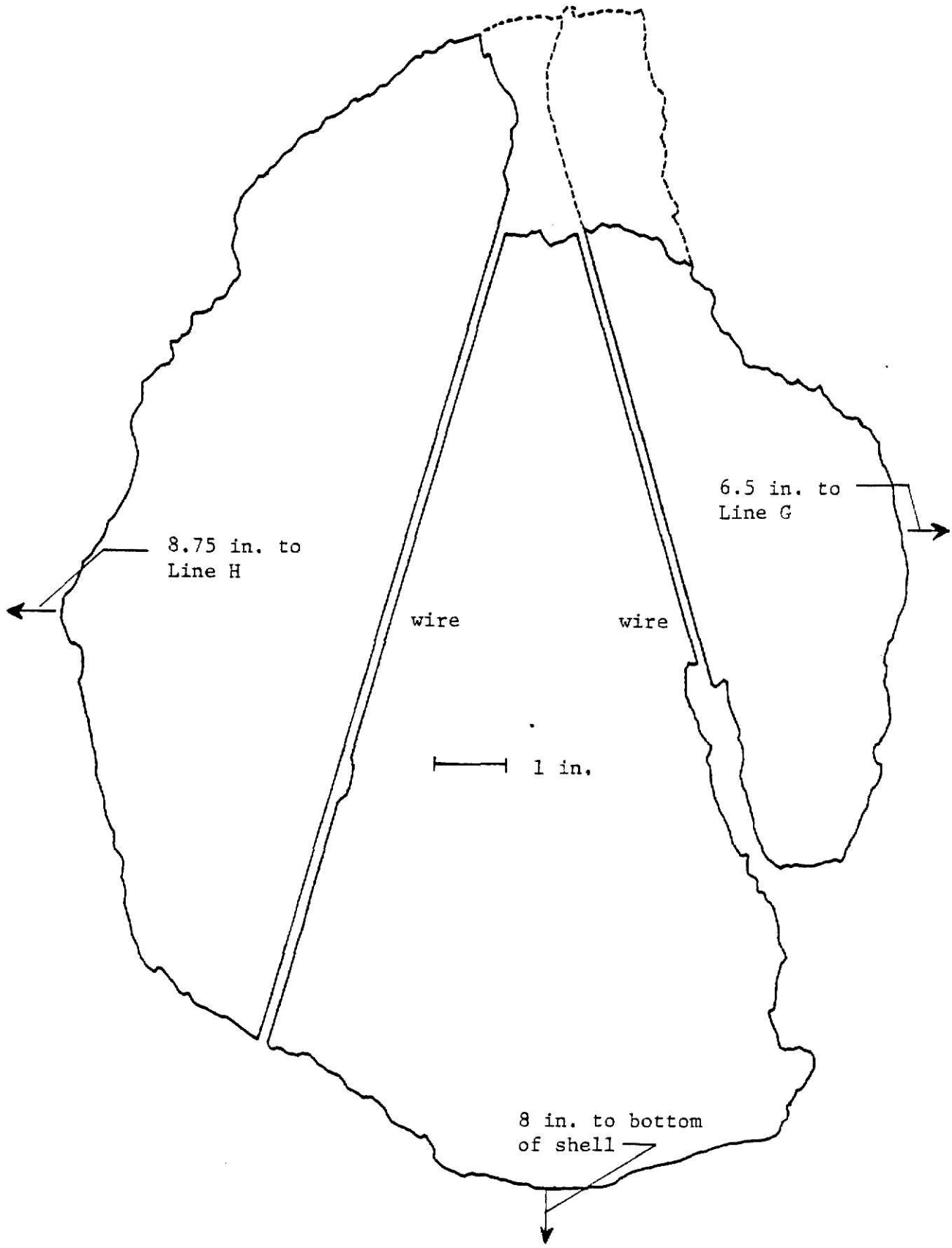

Fig. 16. Outside View of Hole, Shell No. 1

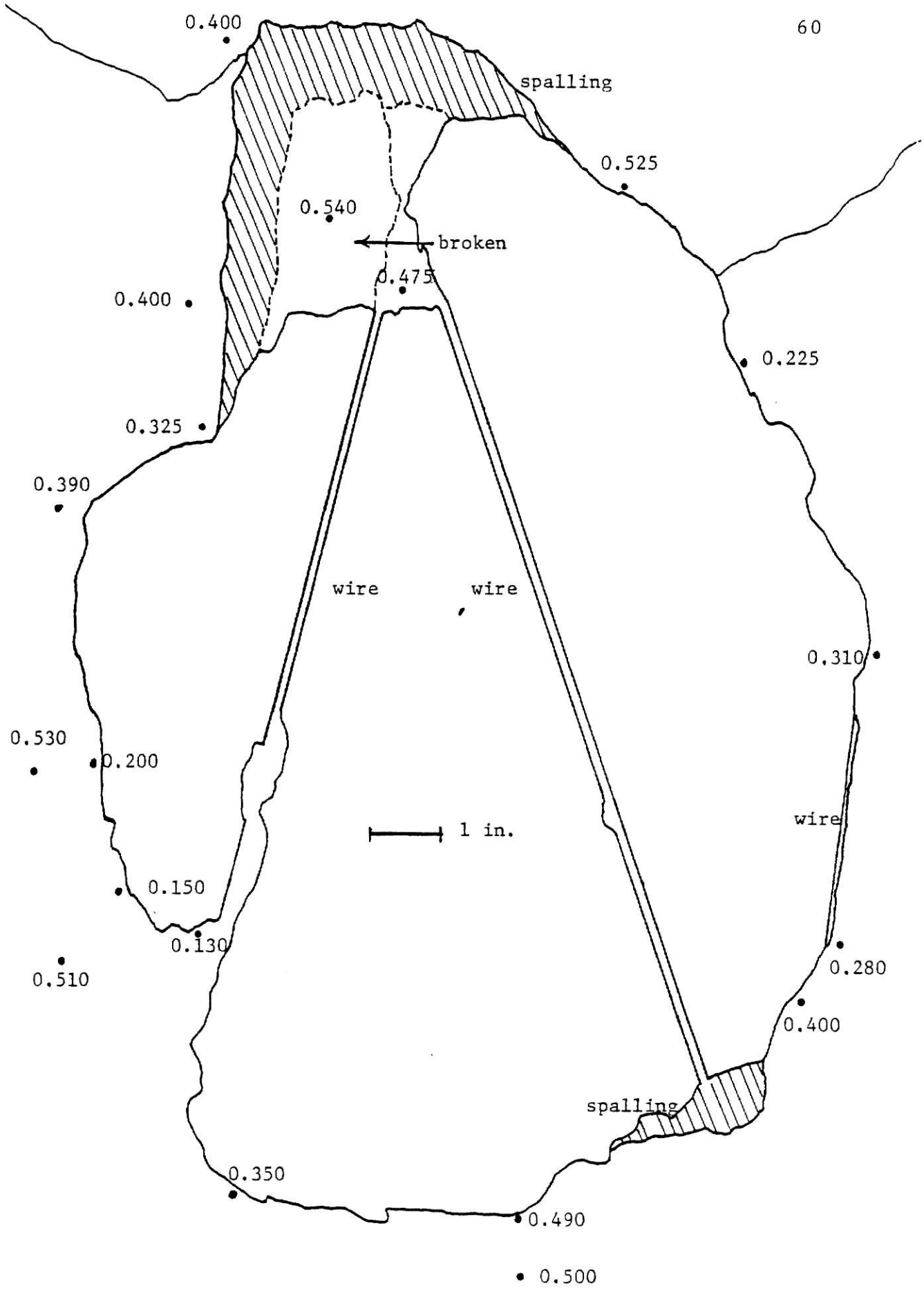

• denotes thickness, in.
1 in. = 25.4mm

Fig. 17. Inside View of Hole, Shell No. 1

Appendix III. : Computer Program

ILLEGIBLE DOCUMENT

THE FOLLOWING DOCUMENT(S) IS OF POOR LEGIBILITY IN THE ORIGINAL

THIS IS THE BEST COPY AVAILABLE

```
      $JOB              ,P=20
      C LNTH,LMPH,THND,THNQ,REFERS TO CIRCULAR SHAPE IMPERFECTION, LNTHS,LMPHS,THNDS
      C THNQS REFERS TO STRAIGHT LINE IMPERFECTION.
      C NPHD IS DUE TO DEAD LOAD NPHQ IS DUE TO UNIT UNIFORM EXTERNAL LOAD, Q=1
      C NPHP,NTHP IS DUE TO LOAD AT TOP OF SHELL
      C POISSON'S RATIO=0.16
      C THE SHELL CARRIES 5/9 OF THE TOP COVER LOAD
    1      DIMENSION R(11),TANPHI(11),PHI(11),XI(11),F(11),ZETA(11),NPHQ(11),
           1 NPHD(11),K(11),KBAR(11),LNTH(11),LMPH(11),LNTHS(11),LMPHS(11),
           2DDELTA(9,12),PERM(9,12),PERM(9,12),NPHP(11),NTHP(11),AEPPH(9,12),
           3PERMS(9,12),PERMS(9,12),AEPTH(9,12),CEPH(9,12),
           4NTHD(11),NTHQ(11),RTH(11),RPH(11),BNTH(9,12),R(11,12),EPSITH(9,12
           5),BNPH(11),BMPH(9,12),SIGMAI(9,12),EPSITS(9,12),SIGMAC(9,12),
           6BNTHS(9,12),BMPHS(9,12),SIGMSI(9,12),SIGMSC(9,12),
           7EPSIPO(9,12),EPSIPI(9,12),EPSISO(9,12),EPSISI(9,12)
           8,SIGMO(9,12),SIGMI(9,12),EPSIC(9,12),EPSII(9,12),
           9ANTH(11),APSITH(11,12),APSIPH(11,12)
    2      REAL NPHQ,NPHD,K,KBAR,LNTH,LMPH,LNTHS,LMPHS,NTHD,NTHQ,NPHP,NTHP
    3      A=36.
    4      RB=56.
    5      HT=108.
    6      B=A*HT/SQRT(RB**2.-A**2.)
    7      TANPHT=-B/A*SQRT(38.7**2./(38.7**2.-36.**2.))
    8      PHT=ATAN2 (TANPHT,1.)
    9       PHT=3.14159+PHT
   10      XIT=SQRT(1+(B/A)**2.)*COS(PHT)
   11      FT=2.*XIT/(1-XIT**2)+ALOG((1+XIT)/(1-XIT))
   12      ZETAT=B**2./(A**2.*SIN(PHT)**2-B**2.*COS(PHT)**2)
   13      READ,(R(I),I=1,11)
   14      DO 3 I=1,11
   15      IF (I.EQ.4) PHI(I)=3.14159/2.
   16      IF(I.EQ.4.) GO TO 5
   17      TANPHI(I)=B/A*SQRT(R(I)**2./(R(I)**2.-A**2.))
   18      IF (I.LE.3) TANPHI(I)=-TANPHI(I)
   19      PHI(I)=ATAN2 (TANPHI(I),1.)
   20      IF (PHI(I).LT.0) PHI(I)=3.14159+PHI(I)
   21    5 XI(I)=SQRT (1+(B/A)**2.)*COS(PHI(I))
   22      F(I)=2.*XI(I)/(1.-XI(I)**2)+ALOG((1.+XI(I))/(1.-XI(I)))
   23      ZETA(I)=B**2/(A**2*SIN(PHI(I))**2-B**2*COS(PHI(I))**2)
   24      NPHQ(I)=-A**2/(2.*B)*SQRT(ZETA(I))/(1+ZETA(I))*(ZETA(I)-ZETAT)
   25      G=.03906
   26      NPHD(I)=-G/4.*B**2*SQRT(A**2+B**2)*SQRT(1-XI(I)**2)/(A**2+B**2
           1 -A**2*XI(I)**2)*(F(I)-FT)
   27      RTOP=38.7
   28      P=1./2.*5./9.*RTOP
   29      NPHP(I)=-RTOP*P/(R(I)*SIN(PHI(I)))
   30      K(I)=(3./(R(I)**2.*.25))**.25
   31      KBAR(I)=(K(I)*24.)/4.
   32      LNTH(I)=2./KBAR(I)*(1-2.*COS(KBAR(I))*EXP(-KBAR(I))+COS(2.*KBAR(I)
           1)*EXP(-2.*KBAR(I)))
   33      LMPH(I)=2./KBAR(I)*(2.*SIN(KBAR(I))*EXP(-KBAR(I))-SIN(2.*KBAR(I))
           1*EXP(-2.*KBAR(I)))
   34      LNTHS(I)=1.-(COS(2.*KBAR(I))+SIN(2.*KBAR(I)))*EXP(-2.*KBAR(I))
   35      NTHD(I)=-G*A**2/(A**2+B**2)**.5*XI(I)/(1.-XI(I)**2)**.5+NPHD(I)*A*
           1*2/B**2*(1.-XI(I)**2)
   36      RTH(I)=R(I)/SIN(PHI(I))
   37      RPH(I)=-A**2*B**2/(A**2*(SIN(PHI(I)))**2-B**2*(COS(PHI(I)))**2)**
           11.5
   38      NTHQ(I)=-RTH(I)/RPH(I)*NPHQ(I)-RTH(I)
   39      NTHP(I)=-RTH(I)/RPH(I)*NPHP(I)
```

```
      3 LMPHS(I)=1.-(COS(2.*KBAR(I))-SIN(2.*KBAR(I)))*EXP(-2.*KBAR(I))
        DO 90 I=1,11
        ANTH(I)=NTHQ(I)+NTHP(I)
   90   BNPH(I)=NPHQ(I)+NPHP(I)
        CALL DVIA(DDELTA)
        E=3.62 E06
        READ,((H(I,J),I=1,11),J=1,12)
        DO 51 J=1,12
        DO 51 I=1,11
        APSITH(I,J)=3.1*(ANTH(I)-0.16*BNPH(I))/(E*H(I,J))
   51   APSIPH(I,J)=3.1*(BNPH(I)-0.16*ANTH(I))/(E*H(I,J))
        PRINT 31,((APSITH(I,J),J=1,6),I=1,11)
        PRINT 32,((APSITH(I,J),J=7,12),I=1,11)
   31 FORMAT (10X,'APSITH=EPSILON THETA BY MEMBRANE THEORY WITH POISSON
     1RATIO = 0.16',//,16X,'A',10X,'B',10X,'C',10X,'D',10X,'E',10X,'F',/
     2/,10X,11(6E11.3,//,10X))
   32 FORMAT (16X,'G',10X,'H',10X,'I',10X,'J',10X,'K',10X,'L',//,10X,11(
     16E11.3,//,10X))
        PRINT 41,((APSIPH(I,J),J=1,6),I=1,11)
        PRINT 42,((APSIPH(I,J),J=7,12),I=1,11)
   41 FORMAT (10X,'APSIPH=EPSILON PHI BY MEMBRANE THEORY WITH POISSON RA
     1TIO = 0.16',//,16X,'A',10X,'B',10X,'C',10X,'D',10X,'E',10X,'F',//,
     210X,11(6E11.3,//,10X))
   42 FORMAT (16X,'G',10X,'H',10X,'I',10X,'J',10X,'K',10X,'L',//,10X,11(
     16E11.3,//,10X))
        DO 50 J=1,12
        DO 50 I=1,9
        L=I+1
        PERN(I,J)=-LNTH(L)*2.*DDELTA(I,J)/24.*K(L)*R(L)*BNPH(L)
        PERNS(I,J)=-LNTHS(L)*2.*DDELTA(I,J)/24.*K(L)*R(L)*BNPH(L)
        PERM(I,J)=-LMPH(L)*2.*DDELTA(I,J)/24./(2.*K(L))*BNPH(L)
   50   PERMS(I,J)=-LMPHS(L)*2.*DDELTA(I,J)/24./(2.*K(L))*BNPH(L)
        DO 60 J=1,12
        DO 60 I=1,9
        L=I+1
        BNTH(I,J)=PERN(I,J)+NTHQ(L)+NTHP(L)
        BNTHS(I,J)=PERNS(I,J)+NTHQ(L)+NTHP(L)
        EPSITH(I,J)=3.1*(BNTH(I,J)-0.16*BNPH(L))/(E*H(L,J))
        EPSITS(I,J)=3.1*(BNTHS(I,J)-0.16*BNPH(L))/(E*H(L,J))
        AEPTH(I,J)=(EPSITH(I,J)+EPSITS(I,J))/2.
        SIGMAO(I,J)=3.1*(BNPH(L)/H(L,J)+PERM(I,J)/(1./6.*H(L,J)**2))
        SIGMAI(I,J)=3.1*(BNPH(L)/H(L,J)-PERM(I,J)/(1./6.*H(L,J)**2))
        SIGMSO(I,J)=3.1*(BNPH(L)/H(L,J)+PERMS(I,J)/(1./6.*H(L,J)**2))
        SIGMSI(I,J)=3.1*(BNPH(L)/H(L,J)-PERMS(I,J)/(1./6.*H(L,J)**2))
        EPSIPO(I,J)=SIGMAO(I,J)/E-0.16*EPSITH(I,J)
        EPSIPI(I,J)=SIGMAI(I,J)/E-0.16*EPSITH(I,J)
        EPSISO(I,J)=SIGMSO(I,J)/E-0.16*EPSITS(I,J)
        EPSISI(I,J)=SIGMSI(I,J)/E-0.16*EPSITS(I,J)
        AEPPH(I,J)=(EPSIPO(I,J)+EPSIPI(I,J)+EPSISO(I,J)+EPSISI(I,J))/4.
        SIGMO(I,J)=(SIGMAO(I,J)+SIGMSO(I,J))/2.
        SIGMI(I,J)=(SIGMAI(I,J)+SIGMSI(I,J))/2.
        EPSIO(I,J)=SIGMO(I,J)/E-0.16*AEPTH(I,J)
        EPSII(I,J)=SIGMI(I,J)/E-0.16*AEPTH(I,J)
   60   CEPH(I,J)=3.1*BNPH(L)/(E*H(I,J))-1.16*AEPTH(I,J)
        PRINT 174,((AEPTH(I,J),J=1,6),I=1,9)
        PRINT 175,((AEPTH(I,J),J=7,12),I=1,9)
  174   FORMAT (10X,'AEPTH=AVERAGE EPSILON THETA, WITH IMPERFECTION',//,16
     1X,'A',10X,'B',10X,'C',10X,'D',10X,'E',10X,'F',//,10X,9(6E11.3,//,1
     20X))
  175   FORMAT (16X,'G',10X,'H',10X,'I',10X,'J',10X,'K',10X,'L',//,10X,9(6
```

```
          1E11.3,//,10X))
 92         PRINT 184,((AEPPH(I,J),J=1,6),I=1,9)
 93         PRINT 185,((AEPPH(I,J),J=7,12),I=1,9)
 94     184 FORMAT (10X,'AEPPH=AVERAGE EPSILON PHI, WITH IMPERFECTION',//,16X,
          1'A',10X,'B',10X,'C',10X,'D',10X,'E',10X,'F',//,10X,9(6E11.3,//,10X
          2))
 95     185 FORMAT (16X,'G',10X,'H',10X,'I',10X,'J',10X,'K',10X,'L',//,10X,9(6
          1E11.3,//,10X))
 96         STOP
 97         END

 98         SUBROUTINE DVIA(DDELTA)
 99         DIMENSION DELTA(11,12),DDELTA(9,12)
100         READ,((DELTA (I,J),I=1,11),J=1,12)
101         DO 100 J=1,12
102         DO 100 I=1,9
103         L=I+1
104         M=I+2
105     100 DDELTA(I,J)=DELTA(L,J)-.5*(DELTA(I,J)+DELTA(M,J))
106         RETURN
107         END
```

```
$ENTRY
APSITH=EPSILON THETA BY MEMBRANE THEORY WITH POISSON RATIO = 0.15

      A           B           C           D           E           F

-0.804E-04 -0.323E-04 -0.891E-04 -0.589E-04 -0.464E-04 -0.667E-04

-0.128E-03 -0.425E-04 -0.524E-04 -0.998E-04 -0.524E-04 -0.743E-04

-0.510E-04 -0.576E-04 -0.740E-04 -0.415E-04 -0.321E-04 -0.536E-04

-0.514E-04 -0.593E-04 -0.934E-04 -0.405E-04 -0.752E-04 -0.481E-04

-0.432E-04 -0.662E-04 -0.818E-04 -0.478E-04 -0.576E-04 -0.478E-04

-0.779E-04 -0.798E-04 -0.103E-03 -0.333E-04 -0.426E-04 -0.359E-04

-0.101E-03 -0.546E-04 -0.792E-04 -0.462E-04 -0.387E-04 -0.411E-04

-0.242E-04 -0.316E-04 -0.305E-04 -0.328E-04 -0.283E-04 -0.412E-04

-0.448E-04 -0.293E-04 -0.293E-04 -0.427E-04 -0.354E-04 -0.338E-04

-0.528E-04 -0.179E-04 -0.154E-04 -0.900E-04 -0.408E-04 -0.373E-04

-0.365E-04 -0.128E-04 -0.157E-04 -0.464E-04 -0.587E-04 -0.330E-04


      G           H           I           J           K           L

-0.733E-04 -0.569E-04 -0.458E-04 -0.647E-04 -0.132E-03 -0.485E-04

-0.103E-03 -0.779E-04 -0.432E-04 -0.665E-04 -0.113E-03 -0.177E-03

-0.364E-04 -0.399E-04 -0.366E-04 -0.536E-04 -0.536E-04 -0.426E-04

-0.670E-04 -0.629E-04 -0.474E-04 -0.505E-04 -0.541E-04 -0.522E-04
```

-0.510E-04 -0.972E-04 -0.527E-04 -0.740E-04 -0.635E-04 -0.451E-04

-0.477E-04 -0.524E-04 -0.515E-04 -0.626E-04 -0.998E-04 -0.409E-04

-0.792E-04 -0.537E-04 -0.512E-04 -0.924E-04 -0.653E-04 -0.456E-04

-0.449E-04 -0.243E-04 -0.242E-04 -0.604E-04 -0.210E-04 -0.274E-04

-0.509E-04 -0.256E-04 -0.652E-04 -0.547E-04 -0.391E-04 -0.620E-04

-0.293E-04 -0.263E-04 -0.501E-04 -0.609E-04 -0.460E-04 -0.489E-04

-0.323E-04 -0.233E-04 -0.542E-04 -0.813E-04 -0.621E-04 -0.418E-04

APSIPH=EPSILON PHI BY MEMBRANE THEORY WITH POISSON RATIO.= 0.16

A	B	C	D	E	F
-0.877E-05	-0.353E-05	-0.972E-05	-0.642E-05	-0.506E-05	-0.749E-05
-0.120E-04	-0.402E-05	-0.494E-05	-0.941E-05	-0.494E-05	-0.700E-05
-0.416E-05	-0.470E-05	-0.604E-05	-0.338E-05	-0.261E-05	-0.437E-05
-0.396E-05	-0.457E-05	-0.720E-05	-0.313E-05	-0.579E-05	-0.371E-05
-0.352E-05	-0.539E-05	-0.667E-05	-0.390E-05	-0.470E-05	-0.390E-05
-0.734E-05	-0.753E-05	-0.971E-05	-0.314E-05	-0.402E-05	-0.358E-05
-0.114E-04	-0.617E-05	-0.897E-05	-0.523E-05	-0.438E-05	-0.405E-05
-0.327E-05	-0.428E-05	-0.413E-05	-0.444E-05	-0.383E-05	-0.568E-05
-0.711E-05	-0.465E-05	-0.465E-05	-0.679E-05	-0.562E-05	-0.537E-05
-0.960E-05	-0.326E-05	-0.280E-05	-0.164E-04	-0.743E-05	-0.673E-05
-0.803E-05	-0.260E-05	-0.318E-05	-0.944E-05	-0.119E-04	-0.671E-05

G	H	I	J	K	L
-0.799E-05	-0.620E-05	-0.499E-05	-0.705E-05	-0.144E-04	-0.529E-05
-0.971E-05	-0.734E-05	-0.407E-05	-0.627E-05	-0.104E-04	-0.167E-04
-0.321E-05	-0.325E-05	-0.298E-05	-0.437E-05	-0.437E-05	-0.347E-05
-0.516E-05	-0.485E-05	-0.365E-05	-0.389E-05	-0.417E-05	-0.403E-05
-0.416E-05	-0.792E-05	-0.430E-05	-0.604E-05	-0.517E-05	-0.367E-05
-0.449E-05	-0.494E-05	-0.486E-05	-0.590E-05	-0.941E-05	-0.386E-05
-0.897E-05	-0.607E-05	-0.579E-05	-0.105E-04	-0.738E-05	-0.516E-05
-0.609E-05	-0.330E-05	-0.327E-05	-0.818E-05	-0.295E-05	-0.371E-05

-0.809E-05 -0.407E-05 -0.104E-04 -0.868E-05 -0.622E-05 -0.984E-05

-0.534E-05 -0.487E-05 -0.912E-05 -0.111E-04 -0.838E-05 -0.889E-05

-0.656E-05 -0.474E-05 -0.110E-04 -0.165E-04 -0.126E-04 -0.850E-05

AEPTH=AVERAGE EPSILON THETA, WITH IMPERFECTION

A	B	C	D	E	F
-0.123E-03	-0.424E-04	-0.503E-04	-0.985E-04	-0.527E-04	-0.728E-04
-0.506E-04	-0.575E-04	-0.745E-04	-0.411E-04	-0.305E-04	-0.543E-04
-0.534E-04	-0.621E-04	-0.943E-04	-0.418E-04	-0.798E-04	-0.503E-04
-0.431E-04	-0.643E-04	-0.805E-04	-0.460E-04	-0.560E-04	-0.464E-04
-0.781E-04	-0.829E-04	-0.105E-03	-0.335E-04	-0.439E-04	-0.368E-04
-0.101E-03	-0.517E-04	-0.773E-04	-0.432E-04	-0.364E-04	-0.381E-04
-0.251E-04	-0.325E-04	-0.299E-04	-0.352E-04	-0.282E-04	-0.447E-04
-0.443E-04	-0.288E-04	-0.282E-04	-0.415E-04	-0.352E-04	-0.333E-04
-0.466E-04	-0.166E-04	-0.157E-04	-0.786E-04	-0.425E-04	-0.366E-04

G	H	I	J	K	L
-0.107E-03	-0.774E-04	-0.444E-04	-0.653E-04	-0.110E-03	-0.184E-03
-0.368E-04	-0.393E-04	-0.360E-04	-0.528E-04	-0.542E-04	-0.409E-04
-0.717E-04	-0.647E-04	-0.500E-04	-0.534E-04	-0.558E-04	-0.556E-04
-0.500E-04	-0.943E-04	-0.498E-04	-0.743E-04	-0.612E-04	-0.438E-04
-0.474E-04	-0.543E-04	-0.513E-04	-0.632E-04	-0.103E-03	-0.420E-04
-0.769E-04	-0.512E-04	-0.494E-04	-0.902E-04	-0.649E-04	-0.446E-04
-0.472E-04	-0.244E-04	-0.252E-04	-0.602E-04	-0.215E-04	-0.286E-04
-0.482E-04	-0.254E-04	-0.621E-04	-0.551E-04	-0.357E-04	-0.643E-04
-0.318E-04	-0.276E-04	-0.539E-04	-0.566E-04	-0.524E-04	-0.435E-04

AEPPH=AVERAGE EPSILON PHI, WITH IMPERFECTION

A	B	C	D	E	F
-0.136E-04	-0.433E-05	-0.561E-05	-0.103E-04	-0.523E-05	-0.774E-05
-0.454E-05	-0.507E-05	-0.643E-05	-0.370E-05	-0.306E-05	-0.461E-05
-0.395E-05	-0.449E-05	-0.763E-05	-0.318E-05	-0.551E-05	-0.367E-05

```
-0.382E-05 -0.611E-05 -0.741E-05 -0.450E-05 -0.532E-05 -0.444E-05
-0.784E-05 -0.758E-05 -0.101E-04 -0.333E-05 -0.409E-05 -0.348E-05
-0.120E-04 -0.703E-05 -0.984E-05 -0.604E-05 -0.502E-05 -0.541E-05
-0.331E-05 -0.437E-05 -0.445E-05 -0.429E-05 -0.405E-05 -0.535E-05
-0.757E-05 -0.496E-05 -0.507E-05 -0.734E-05 -0.595E-05 -0.573E-05
-0.111E-04 -0.363E-05 -0.290E-05 -0.190E-04 -0.753E-05 -0.714E-05

      G          H          I          J          K          L
-0.984E-05 -0.795E-05 -0.417E-05 -0.691E-05 -0.111E-04 -0.168E-04
-0.386E-05 -0.360E-05 -0.331E-05 -0.484E-05 -0.463E-05 -0.402E-05
-0.483E-05 -0.494E-05 -0.354E-05 -0.375E-05 -0.422E-05 -0.380E-05
-0.464E-05 -0.899E-05 -0.510E-05 -0.646E-05 -0.593E-05 -0.417E-05
-0.486E-05 -0.498E-05 -0.523E-05 -0.623E-05 -0.954E-05 -0.397E-05
-0.990E-05 -0.685E-05 -0.645E-05 -0.115E-04 -0.791E-05 -0.565E-05
-0.607E-05 -0.347E-05 -0.329E-05 -0.869E-05 -0.316E-05 -0.373E-05
-0.895E-05 -0.433E-05 -0.114E-04 -0.907E-05 -0.709E-05 -0.998E-05
-0.520E-05 -0.497E-05 -0.896E-05 -0.123E-04 -0.777E-05 -0.102E-04

CORE USAGE      OBJECT CODE=   12288 BYTES,ARRAY AREA=   14312 BYTES,TOTAL
DIAGNOSTICS       NUMBER OF ERRORS=       0, NUMBER OF WARNINGS=
COMPILE TIME=     0.69 SEC,EXECUTION TIME=     1.17 SEC,     11.22.39
```

Appendix IV. : Notations

Notations

a - throat radius

b - shell geometry parameter

D_{ij} - the central line radial deviation from ideal geometry

Dd - the imperfection out of round

dR - the measured deviation from the ideal geometry

dt - the deviation of shell thickness from 0.5 in.

E_c - Young's Modulus of concrete

E_s - modulus of elasticity of steel

f_c' - concrete uniaxial compressive strength

f_y - yield strength of steel

g - dead weight per unit area of surface

H - distance between 3 dial gages = 24 in.

H_T - vertical distance from the throat to the base

i - the gage number

j - the line number

K, $\bar{K}$ - parameter

M - bending moment

m_ϕ - nondimensionalized meridional moment coefficients

N - membrane force

n_θ - nondimensionalized hoop froce coefficients

q - uniform external pressure

q_{cr} - pressure at which buckling commences

R - horizontal radius

R_B - base radius

R_T - top radius

R_0 - meridional curve parameter

S - deviation express in slop

t - the measured shell thickness at the gage location

Z - vertical coordinate

ϕ - meridional direction

θ - circumferencial direction

$\acute{o}$ - the stress

ε - the strain

Δ - the net radial deviation of the shell surface over a gage length

εo - associated strain for concrete

μ- Poisson's Ratio

Acknowledgements

The writer would like to acknowledge the assistance rendered by Dr. Stuart E. Swartz, Professor of Civil Engineering, during the course of the project and preparation of this thesis.

Sincere thanks are also extended to Professor K. K. Hu for his valuable advice and to Dr. Robert Snell, Head, Department of Civil Engineering, for his continual Support.

Appreciation is also due to Mr. Russell L. Gillespie for his help while working in the Civil Engineering Design Shops and to the Department of Civil Engineering for providing the facilities.

The research reported herein was supported in part by the National Science Foundation, Grant ENG-7818415. This support is gratefully acknowledged.

CONSTRUCTION AND TESTING OF A REINFORCED CONCRETE HYPERBOLIC COOLING TOWER MODEL

by

KARL CHIA-CHANG CHIEN

B.S., National College of Marine Science and Technology, 1971

AN ABSTRACT OF A MASTER'S THESIS

Submitted in partial fulfullment of the

requirement for the degree

MASTER OF SCIENCE

Department of Civil Engineering

Kansas State University
Manhattan, Kansas

1983

ABSTRACT

In a thermal power station, heated steam drives the turbogenerator, which produces electric energy. To create an effective heat sink at the end of this process, the steam is condensed and recycled into the boiler. This requires a large amount of cooling water.

In order to avoid thermal pollution of revers, lakes and seashores natural draft cooling towers are effective and popular corrective measures. Hyperbolic, natural-dragt cooling towers continue to be among the largest reinforced concrete thin-shell structures being built.

In the design of large thin shells, stability is a vital concern. However, few buckling experiments have been conducted on concrete or micreconcrete cylinders, hyperboloids, or toroids subjected to lateral axisymmetric or asymmetric pressures.

The experiment carried out here was concerned with a microconcrete hyperboloid of revollution, wall-type shell model. The test was conducted for a simple, non-offset, hyperboloidal shell with essentially uniform thicknes, 0.5 in.(1.27 cm), 12 ft.(3.66 m) high. The shell was 9.33 ft. (2.84 m) and 6 ft.(1.83 m) in diameter at the base and throat respectively.

The objective of this research was to obtain experimental evidence on the buckling behavior of this type of concrtete shell. The construction, testing, data collection and analysis are presented in detail. The effect of imperfections is also discussed.

The shell buckled and failed locally in a mode that was similar to that experienced by unreinforced spherical caps.